

1           **Regulated release of cryptococcal polysaccharide drives virulence and  
2           suppresses immune infiltration into the central nervous system**

3           **Running title: Regulated release of cryptococcal polysaccharide**

4  
5  
6  
7           Steven T. Denham<sup>1</sup>, Surbhi Verma<sup>1</sup>, Raymond C. Reynolds<sup>1</sup>, Colleen L. Worne<sup>1</sup>,  
8           Joshua M. Daugherty<sup>1</sup>, Thomas E. Lane<sup>1</sup>, Jessica C.S. Brown<sup>1,2</sup>

9  
10          <sup>1</sup>Division of Microbiology and Immunology, Pathology Department, University of Utah  
11          School of Medicine, Salt Lake City, UT, USA

12          <sup>2</sup>Correspondence: jessica.brown@path.utah.edu

13  
14  
15  
16  
17  
18  
19  
20  
21  
22  
23  
24  
25  
26  
27  
28  
29  
30  
31  
32  
33  
34  
35  
36  
37  
38  
39  
40  
41  
42  
43  
44  
45

46 **Abstract:**

47       *Cryptococcus neoformans* is a common environmental yeast and opportunistic  
48 pathogen responsible for 15% of AIDS-related deaths worldwide. Mortality primarily  
49 results from meningoencephalitis, which occurs when fungal cells disseminate to the  
50 brain from the initial pulmonary infection site. A key *C. neoformans* virulence trait is the  
51 polysaccharide capsule. Capsule shields *C. neoformans* from immune-mediated  
52 recognition and destruction. The main capsule component, glucuronoxylomannan  
53 (GXM), is found both attached to the cell surface and free in the extracellular space (as  
54 exo-GXM). Exo-GXM accumulates in patient serum and cerebrospinal fluid at  $\mu\text{g/mL}$   
55 concentrations, has well-documented immunosuppressive properties, and correlates  
56 with poor patient outcomes. However, it is poorly understood whether exo-GXM release  
57 is regulated or the result of shedding during normal capsule turnover. We demonstrate  
58 that exo-GXM release is regulated by environmental cues and inversely correlates with  
59 surface capsule levels. We identified genes specifically involved in exo-GXM release  
60 that do not alter surface capsule thickness. The first mutant, *liv7Δ*, released less GXM  
61 than wild-type cells when capsule is not induced. The second mutant, *cnag\_00658Δ*,  
62 released more exo-GXM under capsule-inducing conditions. Exo-GXM release  
63 observed *in vitro* correlated with polystyrene adherence, virulence, and fungal burden  
64 during murine infection. Additionally, we find that exo-GXM reduces cell size and  
65 capsule thickness in capsule-inducing conditions, potentially influencing dissemination.  
66 Finally, we demonstrated that exo-GXM prevents immune cell infiltration into the brain  
67 during disseminated infection and highly inflammatory intracranial infection. Our data

68 suggest that exo-GXM performs a different role from capsule GXM during infection,  
69 altering cell size and suppressing inflammation.

70

71 **Introduction:**

72       *Cryptococcus neoformans* is a globally distributed saprophytic fungus found  
73 associated with certain species of trees and bird droppings (1). Due to its global  
74 environmental distribution, human exposure to *C. neoformans* is almost universal (1, 2).  
75 Exposure occurs via inhaled fungal spores or desiccated yeast cells enter the lungs,  
76 where they are either cleared by the immune system, or contained in a persistent state  
77 for a decade or more (3). However, in immunocompromised hosts *C. neoformans* cells  
78 can disseminate from the lungs to basically any organ in the body (4). *C. neoformans*  
79 proliferates particularly well in the brain, resulting in life-threatening meningoencephalitis  
80 (5). Cryptococcal infections are responsible for 15% of acquired immune deficiency  
81 syndrome (AIDS) related deaths worldwide, with meningoencephalitis being the primary  
82 cause of death. (6). Most cases occurring in sub-Saharan Africa and Asia, with mortality  
83 rates exceeding 50% in resource poor areas (6).

84       In contrast to many forms of bacterial and viral meningitis, cryptococcal  
85 meningoencephalitis is associated with strikingly low levels of inflammation and  
86 infiltrating immune cells into the central nervous system (CNS) of both human patients  
87 and mouse models (7-11). This paucity of inflammation is linked to poorer clinical  
88 outcomes, and subdued clinical signs that can delay treatment (9, 12, 13).

89       An essential factor for *C. neoformans* virulence is the conditional production of a  
90 thick polysaccharide surface capsule, which can more than double the diameter of a *C.*

91     *neoformans* cell (14). The primary capsule constituent is glucuronoxylomannan (GXM),  
92     which comprises approximately 90% of the capsule mass (15, 16). Surface capsule  
93     plays a number of different roles during pathogenesis, protecting *C. neoformans* cells  
94     from phagocytosis, complement, and oxidative stress (15, 17, 18). GXM also has  
95     numerous immunomodulatory properties that facilitate fungal survival in the host (19).  
96     Notably, GXM increases anti-inflammatory cytokine (IL-10) release while dampening  
97     proinflammatory cytokine release (IL-12, IFN- $\gamma$ , TNF- $\alpha$ , IL-1B and IL-6) (20-23). GXM  
98     disrupts antigen presentation by macrophages and dendritic cells, and can even induce  
99     macrophage apoptosis, thereby diminishing T cell proliferation (21, 24-26). GXM can  
100    also suppress leukocyte infiltration into sites of inflammation (27-29).

101       GXM is non-covalently attached to the cell surface during cell surface capsule  
102     formation and maintenance (16). It is also found free within the extracellular milieu. This  
103     exo-cellular GXM (exo-GXM) reaches mg/mL concentrations in laboratory growth  
104     medium (30), and can be observed in the high  $\mu$ g/mL range in patient serum and  
105     cerebrospinal fluid (10, 31). GXM serum titers in HIV-associated cryptococcosis patients  
106     positively correlate with non-protective immune signatures and increased mortality (32).

107       Despite longstanding knowledge of the existence of exo-GXM, its connection to  
108     cell-associated GXM and the mechanisms behind its release remain largely unclear.  
109     One hypothesis has been that exo-GXM is shed mechanically from the cell surface  
110     capsule (16, 33). Alternatively, it has been speculated that distinct mechanisms might  
111     regulate the production of cell-associated and exo-GXM in response to environmental  
112     cues (15, 16, 34). This latter hypothesis is supported by observations that cell-  
113     associated and exo-GXM display different biophysical properties (34). Decreased

114 electromobility of exo-GXM under capsule inducing conditions indicates that these  
115 differences could occur at the level of polymer length or branching (35-37).  
116 Here we test the hypothesis that exo-GXM production is regulated by  
117 environmental conditions. We find that exo-GXM production is inversely related to the  
118 thickness of the cell surface-retained capsule and identify genes involved in these  
119 processes. Exo-GXM production also correlates with virulence and reduces infiltration of  
120 immune cells into the CNS during infection. Together, these data support the idea that  
121 exo-GXM plays a critical but distinct role from cell surface GXM during infection.

122

123 **Results:**

124 Environmental signals alter exo-GXM levels

125 To investigate whether exo-GXM release is passive shedding of surface capsule  
126 or regulated at some level, we cultured wild-type *C. neoformans* cells for 24 hours under  
127 a variety of media conditions. We then measured capsule size and exo-GXM released  
128 into the medium. We chose both non-capsule inducing media and a series of capsule  
129 inducing media intended to produce a range of capsule induction. We harvested cells,  
130 then stained with india ink to measure capsule thickness as the distance from the cell  
131 wall to the outer capsule edge (**Fig. 1A**). We filtered supernatant through a through a  
132 0.22 µm filter to remove cells, then immunoblotted with the α-GXM monoclonal antibody  
133 (mAb) F12D2 to quantify exo-GXM release as relative staining intensity (**Fig. 1B**). Exo-  
134 GXM band intensities were normalized to yeast nitrogen base (YNB) + 2% glucose  
135 levels, which was the condition with the greatest observed levels of exo-GXM.

136 We found an inverse relationship between capsule thickness and exo-GXM, such  
137 that cells growing in the strongest capsule inducing conditions, like 10% Sabouraud's  
138 buffered to alkaline pH, produced the least amount of exo-GXM (**Fig. 1B,C**). This  
139 relationship held across other capsule inducing conditions, such as nitrogen and iron  
140 limitation, that produce intermediate levels of both cell surface and exo-GXM.

141 GXM is an  $\alpha$ -1,3-mannan backbone with branching glucuronic acid and xylose  
142 residues and variable 6-O-acetylation on the backbone (38). O-acetylation varies across  
143 strains, is not required for capsule formation, but significantly affects GXM's  
144 immunoreactive properties (38-40). Deletion of CAS1, which is required for O-  
145 acetylation, results in a hypervirulent phenotype (41). We analyzed the same  
146 conditioned media as in **Figure 1**, but used the mAb 1326 to detect GXM. MAb 1326  
147 recognizes O-acetyl (+) GXM, but is unable to recognize O-acetyl (-) GXM. F12D2, on  
148 the other hand, recognizes both O-acetyl (+) and (-) GXM. Thus, 1326 staining intensity  
149 relative to F12D2 intensity reflects the relative proportion of O-acetyl (+) GXM present in  
150 the supernatant. We observed that 1326 staining relative to F12D2 staining increased  
151 under certain capsule inducing conditions (low nitrogen, low iron, and 10% Sabouraud's,  
152 pH 5-6), indicative of increased O-acetylated GXM (**Fig. S1**). These results demonstrate  
153 that environmental conditions may also influence GXM modification, specifically O-  
154 acetylation, with potential implications for immune recognition.

155

156 *Identification of gene deletion mutants with reduced exo-GXM secretion under non-*  
157 *capsule inducing conditions.*

158 We then identified mutants with reduced GXM production. We screened the *C.*  
159 *neoformans* partial knockout collection (CM18 background, 1200 targeted gene  
160 knockouts) (42) under YNB, which results in high exo-GXM production. We grew each  
161 strain for 24 hours at 37°C, removed the cells by centrifugation, then probed the  
162 conditioned medium for exo-GXM.

163 We searched the YNB-grown mutants for samples that produced less exo-GXM  
164 than wild-type cells. We then stained induced cell surface capsule (by growth in 10%  
165 Sabouraud's, pH 7.3) in this subset of mutants and eliminated any with a growth defect  
166 and/or a substantial reduction (>25%) reduction in cell surface capsule thickness. We  
167 also stained for common pathogen-associated molecular patterns (PAMPs), such as  
168 exposed mannoproteins and chitin, which activate host immune responses (43). This  
169 left us with a single mutant, *cnag\_06464Δ*, or *liv7Δ*, which we re-constructed in the  
170 KN99 genetic background (**Fig. 2**). Four other mutants (**Table S1**) exhibited a moderate  
171 defect in cell surface capsule in addition to their moderate defects in exo-GXM release.  
172 However, we focused on the *liv7Δ* mutant because of its ability to form wild-type levels  
173 of cell surface capsule.

174 The *LIV7* gene was previously identified in a screen for mutants deficient in  
175 competitive growth in the lungs after being pooled with 47 other gene deletion mutants  
176 (42). *Liv7* is localized to the Golgi under capsule-inducing conditions (DMEM + 5% CO<sub>2</sub>)  
177 (44). *liv7Δ* cells produce wild-type-like levels of cell surface capsule when grown in 10%  
178 Sabouraud's, pH 7.3 (**Fig. 2A,B**), but conditioned medium from *liv7Δ* cell cultures grown  
179 in YNB contains two-fold less GXM than conditioned medium from wild-type *C.*

180 *neoformans* cell cultures (**Fig. 2C,D**). PAMP exposure is comparable to wild-type cells  
181 (**Fig. S2A,B**).

182 The environment within the host is highly variable, and capsule sizes within  
183 different host niches also vary. While capsule is strongly induced in the lungs, capsule  
184 size varies considerably between strains and throughout infection (45, 46), including  
185 during phagocytosis by macrophages (45). We were interested in whether *liv7Δ* cells  
186 also released less exo-GXM under any capsule inducing conditions. We did observe a  
187 reduction in exo-GXM release by *liv7Δ* cells in low nitrogen media (YCB+0.5g/L urea),  
188 which results in mild capsule induction (**Fig. 1C**, **Fig. 2E,F**).

189 We also took measures to ensure that the relative levels of exo-GXM analyzed  
190 by immunoblotting reflected the actual abundance of exo-GXM in culture supernatant,  
191 rather than a change in GXM's antigenicity. We purified GXM from the supernatant of  
192 wild-type and *liv7Δ* cells grown for 72 hours in YNB. Not only did we purify half as much  
193 exo-GXM from *liv7Δ* cells as wild-type cells (**Fig. 2G**), but after immunoblotting an equal  
194 mass of wild-type and *liv7Δ* cell exo-GXM, we did not detect a substantial difference in  
195 signal intensity (**Fig. 2H,I**).

196

197 Identification of gene deletion mutants with elevated exo-GXM secretion under strong  
198 capsule inducing conditions.

199 We next identified mutants that produced elevated levels of exo-GXM under  
200 capsule-inducing conditions, when exo-GXM production is very low. We again screened  
201 the *C. neoformans* knockout mutant collection (CM18 background), this time growing  
202 the mutants in YNB, then subculturing by diluting 1/100 into 10% Sabouraud's, pH 7.3,

203 and growing 48 hours at 37°C. We again removed mutants that exhibited growth  
204 defects, elevated PAMP exposure, and a substantial reduction (>25%) reduction in cell  
205 surface capsule thickness. We found two groups of mutants: group #1 exhibited  
206 approximately wild-type capsule thickness, while group #2 mutants had less-than-wild-  
207 type levels of cell surface capsule (**Table S1**). We focused our subsequent experiments  
208 on the mutant in gene *cnag\_00658*, which produces cell surface capsule with the same  
209 thickness as wild-type cells (**Fig. 3A,B**). The *CNAG\_00658* gene was previously  
210 screened for competitive growth in the lungs as part of a pooled infection with 47 other  
211 mutant strains, but did not display a significant competitive advantage or disadvantage  
212 (42). As with *liv7Δ*, we re-constructed this mutant in the KN99 genetic background and  
213 used those strains for all subsequent experiments. As in the CM18 background, *cnag-*  
214 *\_00658Δ* cells in the KN99 background released increased exo-GXM in 10%  
215 Sabouraud's, pH 7.3 (**Fig 3C,D**). Under non-capsule inducing conditions (YNB+2%  
216 glucose), *cnag\_00658Δ* cells released wild-type equivalent levels of exo-GXM (**Fig.**  
217 **3E,F**). Unlike other mutants in group #1, *cnag\_00658Δ* cells produce the same levels of  
218 melanin and urease as wild-type cells (**Fig. S2C**).

219 We examined whether the observed immunoblot intensities for GXM produced by  
220 *cnag\_00658Δ* cells were truly due to differences in total abundance and not any  
221 potential effects the *CNAG\_00568* gene might have on GXM's antigenicity. We grew  
222 wild-type and *cnag\_00658Δ* cells for 72 hours in 10% Sabouraud's pH 7.3, but were not  
223 able to successfully purify enough GXM from our 50 mL cultures for immunoblotting,  
224 perhaps because little exo-GXM is released under strong capsule inducing conditions,  
225 such as 10% Sabouraud's pH 7.3 (**Fig 1C, Fig3C**).

226       The *CNAG\_00658* gene encodes a predicted protein 624aa in length. It shares  
227       N-terminal sequence homology with the *Schizosaccharomyces pombe* inner nuclear  
228       membrane protein, IMA1 (615aa). *CNAG\_00658*'s predicted gene product also has five  
229       putative transmembrane domains that positionally align with the 5 transmembrane  
230       domains of the *S. pombe* IMA1 protein. For these reasons, we propose to rename the  
231       *CNAG\_00658* gene "IMA1".

232

233 *Changes in exo-GXM levels alter fungal cell adherence.*

234       We had thus far only assayed exo-GXM secretion during planktonic growth.  
235       However, within its natural environment of soil and vegetable matter, *C. neoformans*  
236       can form adherent biofilms (47). Previous work on cryptococcal biofilms has revealed  
237       that a significant portion of the extracellular matrix is composed of GXM, and that it  
238       plays a critical role in adherence (48). Acapsular strains are unable to adhere to  
239       surfaces such as polystyrene, and the addition of anti-GXM antibodies to developing  
240       wild-type biofilms reduces their adherence (48). We speculated that exo-GXM may be  
241       incorporated into the extracellular matrix during sessile growth to provide community  
242       level structure, and that our exo-GXM mutants would display varying adherence  
243       corresponding to their exo-GXM secretion profiles.

244       To test this, we grew cells at a concentration of  $10^6$  cells/100ul in 96 well  
245       polystyrene plates at 37°C. After 48 hours, the wells were washed forcefully with  
246       PBS+0.1% tween-20 dispensed from an automated plate washer, resuspended in PBS  
247       containing XTT/menadione and left for 5 hours at 37°C. XTT is reduced by fungal cells

248 to produce a colorimetric measure of metabolism that is highly correlative with viable  
249 cell count (49).

250 Wild-type, *cap60Δ*, *liv7Δ#1 / #2*, and *ima1Δ#1 / #2* cells were assayed in both  
251 YNB and 10% Sabouraud's pH 7.3 to replicate planktonic non-capsule and capsule-  
252 inducing conditions respectively. The *cap60Δ* cells served as a negative control, as  
253 acapsular mutants are unable to adhere, likely due to their lack of surface and exo-GXM  
254 (48). We hypothesized that *liv7Δ#1 / #2* cells would display reduced adherence in our  
255 assay due to the reduction in exo-GXM release we observed during planktonic growth.  
256 This was indeed the case, as we observed an approximately two-fold reduction in the  
257 ability of *liv7Δ#1 / #2* cells to adhere in our assay (**Fig. 4A**).

258 In contrast to YNB, *liv7Δ#1 / #2* cells were able to adhere at wild-type levels  
259 when grown in 10% Sabouraud's pH 7.3, perhaps because our observations of  
260 planktonic cells indicated that far less exo-GXM is released by both wild-type and  
261 *liv7Δ#1 / #2* cells under these conditions (**Fig 4B**). Similarly, *ima1Δ#1 / #2* cells, which  
262 displayed elevated exo-GXM release under strong capsule inducing conditions,  
263 demonstrated six to eight-fold higher adherence than wild-type when grown in 10%  
264 Sabouraud's pH 7.3 (**Fig 4B**). When grown in YNB, *ima1Δ#1 / #2* cells still displayed  
265 increased adherence, but it was reduced to an approximately two-fold increase over  
266 wild-type (**Fig 4A**). Moreover, the addition of purified GXM restored *liv7Δ#1 / #2* cell  
267 adherence back to wild-type levels in a concentration-dependent manner (**Fig. 4C**).  
268 Altogether, these results suggest that the regulated secretion of exo-GXM may have a  
269 specialized role in an environmental setting by promoting the adherence of *C.*  
270 *neoformans* communities.

271

272 Host survival and fungal burden correlates with *in vitro* exo-GXM levels.

273 Next, we sought to use *liv7Δ#1 / #2* and *ima1Δ#1 / #2* as an opportunity to  
274 explore roles for exo-GXM during pathogenesis. We hypothesized that exo-GXM  
275 release would promote virulence through its immunomodulatory properties. Since  
276 *liv7Δ#1 / #2* and *ima1Δ#1 / #2* cells produce wild-type sized surface capsules in culture,  
277 we anticipated that *liv7Δ#1 / #2* and *ima1Δ#1 / #2* cells would allow us to assess the  
278 role of exo-GXM in pathogenesis, independent of surface capsule. We predicted that  
279 the reduction of *liv7Δ#1 / #2* cells' ability to produce exo-GXM *in vitro* would result in  
280 reduced virulence. Similarly, we predicted that *ima1Δ#1 / #2* cells, which show  
281 increased exo-GXM under capsule inducing conditions, would display heightened  
282 virulence.

283 We employed a murine model of disseminated cryptococcosis by inoculating  
284 C57BL/6NJ mice (Jackson Labs) intranasally with  $2.5 \times 10^4$  fungal cells per mouse. We  
285 calculated survival as the time it took each mouse to reach 85% of their initial mass.  
286 Consistent with our hypothesis, *in vitro* exo-GXM production inversely correlated with  
287 host-survival. Wild-type KN99 infected mice reached endpoint a median of 20 days  
288 post-inoculation (dpi). In contrast, *liv7Δ#1 / #2*-infected mice reached endpoint a median  
289 of 22.5 dpi, and *ima1Δ#1 / #2*-infected mice a median of 18 dpi (**Fig. 5A**). We observed  
290 similar survival trends when we inoculated C57BL/6NJ mice with ten-fold fewer  
291 cryptococcal cells (**Fig S3A**), or when we inoculated genetically distinct BALB/cJ mice  
292 with the exo-GXM mutant strains (**Fig. S3B**). However, it is important to note that all  
293 strains were sufficiently virulent to cause lethal infection. This was not altogether

294 unexpected, as the exo-GXM secretion phenotypes for *liv7Δ#1 / #2* and *ima1Δ#1 / #2*  
295 cells were dependent on growth conditions, and manifested as a gradient of exo-GXM  
296 production rather than complete ablation or overexpression.

297 We also assessed fungal burden by plating homogenized organs for colony  
298 forming unit (CFU) counts. Organ fungal burden followed the same trends as survival.  
299 Mice inoculated with *liv7Δ#1 / #2* cells consistently presented with lower fungal burden  
300 in the lungs by day 10 post-inoculation (**Fig. 5B**). Dissemination of *liv7Δ#1 / #2* cells to  
301 the spleen (**Fig. S3D**) and brain (**Fig. 5C**) was also reduced compared to wild-type. In  
302 contrast, mice inoculated with *ima1Δ#1 / #2* cells suffered higher pulmonary fungal  
303 burden compared to those inoculated with wild-type *C. neoformans* as early as 3 days  
304 post-inoculation (**Fig. 5D**). We also observed a greater number of disseminated  
305 *ima1Δ#1 / #2* cells in the liver and spleen throughout the course of infection (**Fig.**  
306 **S3E,F**). *ima1Δ#1 / #2* cells disseminated to the brain earlier than wild-type cells, with  
307 some *ima1Δ#1 / #2* CFUs appearing in the brain as early as 3 dpi (**Fig 5E**). Total brain  
308 fungal burden in *ima1Δ#1 / #2* infected mice trended higher than wild-type, with one  
309 independent gene deletion strain achieving a statistically significant increase in fungal  
310 burden 10 dpi and beyond, despite high variance in dissemination at the observed time  
311 points (**Fig. 5E**). These results suggest that time-to-endpoint for the mice was at least  
312 partially due to fungal lung burden and extrapulmonary dissemination, both of which  
313 correlated with *in vitro* exo-GXM release.

314 Since *in vitro* exo-GXM production by *ima1Δ#1 / #2* and *liv7Δ#1 / #2* cells  
315 correlated with virulence *in vivo*, we examined whether or not the *in vitro* phenotypes  
316 would translate to detectable differences in exo-GXM production in the host

317 environment. We analyzed the levels of GXM in the lungs, livers, spleens and brains of  
318 infected mice by performing GXM ELISA's on 0.22  $\mu$ m-filtered organ homogenates.  
319 Exo-GXM levels *in vivo* were highly variable, perhaps reflecting the heterogeneous host  
320 environment or assay insensitivity (**Fig. S4**). In spite of this variability, we detected  
321 significant reductions in total exo-GXM in the lungs and extrapulmonary organs of  
322 *liv7Δ#1 / #2* infected mice at certain time points, with these trends becoming more  
323 apparent as infection progressed (**Fig. S4A-D**). Similarly, *ima1Δ#1 / #2* infected mice  
324 displayed increased total exo-GXM in the lungs, spleen and liver by 14 dpi (**Fig. S4E-G**).  
325 We did not observe any interpretable differences in exo-GXM levels on a per cell basis  
326 (data not shown), possibly due to changing host conditions over the course of  
327 dissemination (46, 50, 51). For instance, GXM per CFU fluctuated greatly in the lungs  
328 and extrapulmonary organs over the course of infection (**Fig. S5A,B**). Spread and/or  
329 clearance of exo-GXM within the host likely also affects these analyses, as the spleen  
330 and livers of infected mice had massively increased exo-GXM levels early in infection,  
331 when few cryptococcal cells had disseminated to those organs (**Fig. S5C**).

332 In addition, we detected exo-GXM in extrapulmonary organs prior to consistent  
333 detection of colony forming units (CFU) in those same organs (**Fig. S5C,D**). This  
334 observation may be relevant for diagnosticians interested in detecting cryptococcal  
335 infection prior to dissemination in at-risk patient populations, as early diagnosis of  
336 cryptococcosis greatly improves outcomes (52).

337

338 *Cell size shifts dramatically during the course of infection in parallel to increases in exo-*  
339 *GXM.*

340 We investigated whether or not *in vitro* capsule phenotypes for the mutants were  
341 recapitulated *in vivo*. We isolated cryptococcal cells from infected mice, fixed them with  
342 paraformaldehyde, and measured cell body diameter, cell surface capsule thickness,  
343 and total diameter (cell diameter including capsule) using india ink (**Fig. 1A**).

344 In wild-type-infected mice, cell and capsule size in the lungs was a broad  
345 distribution that shifted significantly over the course of infection, as observed by others  
346 (53-55). Large cells were abundant early in infection, particularly at 3 dpi (**Fig. 6A**).  
347 These cells were likely Titan cells, which are large, highly polyploid, and increase their  
348 size and ploidy through non-mitotic genome replication (14). However, as infection  
349 progressed, the frequency of large cells decreased. By 20 dpi, smaller cells around  
350 10µm in total diameter dominated the lungs in number (**Fig. 6A**). The cell body size and  
351 capsule thickness distributions experienced proportional shifts, such that overall cell  
352 size to capsule thickness ratios were maintained (**Fig. S6A,B**). In the brain, the  
353 distribution of cell and capsule size was much narrower and overlapped with the  
354 population of smaller cells in the lungs (**Fig. 6B**).

355 When we compared the total cell diameter distributions of wild-type and the exo-  
356 GXM mutants in the lungs, there was no difference 3 dpi (**Fig. 6C,D**). However, by an  
357 early time point in dissemination (14 dpi) the frequency of smaller cells was lower in  
358 *liv7Δ#1 / #2* infected mice, and higher in *ima1Δ#1 / #2* infected mice, when compared to  
359 wild-type-infected mice (**Fig. 6E,F**). The ratio of cell size to capsule thickness was  
360 similar amongst all strains (**Fig. S6C**).

361 Due to this correlation between cell and capsule size and exo-GXM, we  
362 hypothesized that exo-GXM could influence cell and capsule size. To test this, we grew

363 cells in strong cell surface capsule-inducing medium (10% Sabouraud's, pH 7.3) with  
364 minimal exo-GXM release. After 24 hours growth at 37°C, we diluted the cultures 1:2 in  
365 fresh medium and added 100 ng/ml, 10 µg/ml, or 50 µg/ml of purified GXM. After an  
366 additional 24 hours growth, we measured cell and capsule size. We found that both  
367 capsule thickness (**Fig. 7A**) and cell size (**Fig. S7A**) decreased in a dosage-dependent  
368 manner. The greatest decrease was in capsule thickness, which showed a decrease  
369 from a median of 4 µm in control cultures to 1.5 µm in cultures treated with 50 µg/ml  
370 GXM, a decrease of 62.5%. 100 ng/ml showed a more modest decrease, to a median  
371 capsule thickness of 3.6 µm (a 10% decrease). 50 µg/ml and 10 µg/ml GXM treatments  
372 also resulted in a change in cell size, from a median of 6.0 µm for untreated cells to 4.5  
373 µm and 5.3 µm, respectively. 100 ng/ml GXM did not result in a decrease in cell size  
374 (**Fig. S7A**), despite the observed change in capsule thickness (**Fig. 7A**).

375 GXM purification can result in contamination by detergents from the purification  
376 protocol (30). Thus, we performed the same experiment, but added conditioned medium  
377 (from a YNB-grown culture) instead of purified GXM. 20%, 10%, or 1% final  
378 concentration of conditioned medium resulted in decreases in both capsule thickness  
379 and cell size (**Fig. 7B**, **Fig. S7B**). These capsule and cell size changes also depended  
380 on growth: if we did not add fresh medium along with purified GXM, capsule thickness  
381 and cell size did not change (**Fig. S7C,D**).

382 Altogether, these data suggest that changes to exo-GXM release observed *in*  
383 *vitro* can affect pathogenesis. Total exo-GXM released throughout infection correlated  
384 with decreased survival, increased fungal burden and more rapid generation of smaller

385 (haploid) cells in the lungs, which appear more likely to disseminate due to their  
386 dominant presence in extrapulmonary organs.

387

388 **Exo-GXM limits innate immune cell infiltration into the brain.**

389 In human patients, cryptococcal meningoencephalitis is associated with a striking  
390 paucity of inflammation (9). The main driver of mortality, particularly in  
391 immunocompromised patients, is thought to be excessive fungal burden and GXM  
392 accumulation within the CNS, which leads to a devastating increase in intracranial  
393 pressure (10). C57BL/6NJ mice infected with the highly virulent KN99 strain display  
394 similarly limited brain inflammation, despite significant fungal presence. For instance,  
395 when we histologically compared the brains of KN99 infected mice to mock-infected  
396 animals, we could detect very little sign of infiltrating immune cells by H&E staining in  
397 KN99-infected mice, despite local presence of fungi (**Fig. S8**). This was true both early  
398 (14 dpi) (**Fig. S8A,B**) and late (21 dpi) in disseminated infection (**Fig. S8C,D**).  
399 Considering its immunosuppressive nature, we hypothesized that GXM could very likely  
400 play a role in limiting brain inflammation during infection. We correspondingly reasoned  
401 that infection with *liv7Δ#1 / #2* cells might result in increased immune infiltration into the  
402 brain, due to *liv7Δ#1 / #2* cell's reduced exo-GXM secretion.

403 In order to address this hypothesis, we harvested the brains of wild-type and  
404 *liv7Δ#1 / #2* infected animals at 20 days post-intranasal inoculation and analyzed  
405 immune infiltration into the brain via flow cytometry. CD4+ (**Fig. 8A**) and CD8+ (**Fig. 8B**)  
406 cells were scarce in both wild-type and *liv7Δ#1 / #2*-infected brains. These data suggest  
407 that T cells do not significantly respond to brain invasion by *C. neoformans*. Innate

408 immune cells (macrophages/neutrophils) did show some response to wild-type *C.*  
409 *neoformans* cells in the brain, but it was only slightly elevated when compared to mock-  
410 infected animals (**Fig. 8C,D**). This is in stark contrast to bacterial or viral meningitis,  
411 which often show high levels of infiltrating neutrophils and macrophages (7, 8).  
412 Infiltration of both macrophages and neutrophils was increased in *liv7Δ#1 / #2* infected  
413 brains (**Fig. 8C,D**). These results suggest that exo-GXM likely plays an important role in  
414 brain immunosuppression that is independent of surface capsule.

415 We next sought to determine if exo-GXM was sufficient to suppress immune  
416 infiltration into the brain if we induced brain inflammation by direct intracranial  
417 inoculation. We purified GXM from YNB-grown cultures using standard methods (30).  
418 Since we detected GXM associated with the brain up to five days prior to the  
419 appearance of CFU (**Fig. S5**), we administered 200 µg of purified GXM daily by  
420 intraperitoneal injection, beginning five days prior to inoculation (**Fig. 9A**). Additional  
421 mice were administered sterile PBS as a control. We then inoculated mice intracranially  
422 with either wild-type KN99 or acapsular *cap60Δ* cells. Unsurprisingly, *cap60Δ* cells  
423 elicited greater numbers of immune infiltration into the brain (**Fig. 9B,C**), and achieved a  
424 significantly lower fungal burden than wild-type *C. neoformans* (**Fig. 9D**). However,  
425 administration of GXM to mice infected with *cap60Δ* cells reduced immune infiltration  
426 (CD45<sup>hi</sup> cells) into the brain (**Fig. 9B,C and Fig. S9**), and increased fungal burden when  
427 compared to PBS-treated mice (**Fig. 9D**). These results demonstrate that in the context  
428 of an inflammatory infection, exo-GXM is sufficient to promote fungal survival in the  
429 brain, likely through the suppression of brain immune infiltration.

430

431 **Discussion:**

432 Surface capsule is critical for *C. neoformans* virulence. However, GXM that is not  
433 attached to the cell surface, or exo-GXM, accumulates to significant levels in laboratory  
434 culture and during infection (10, 30, 31). Our data strongly suggest that *C. neoformans*  
435 inversely regulates surface capsule formation and exo-GXM release according to  
436 environmental cues. Within our tested conditions, GXM was constitutively produced but  
437 alternately retained at the cell surface or released into the extracellular milieu (**Fig. 1**).

438 We also observed that O-acetylation of GXM's mannose backbone changes with  
439 environmental conditions (**Fig. S1**). Previous findings have also indicated that exo-GXM  
440 release might be an active process. For instance, a study comparing the properties of  
441 exo-GXM and capsular GXM showed that despite identical sugar composition, capsular  
442 GXM and exo-GXM manifested distinct biophysical and antigenic properties (34).

443 Differential regulation of surface capsule and exo-GXM could occur at the level of  
444 GXM polymer length and/or other modification (35-37). Another possibility is that exo-  
445 GXM release is regulated by changing levels of alpha-glucan, which anchors GXM to  
446 the cell surface (56), or by altering release of exosomes containing GXM (57). Either  
447 way, changes in GXM levels, distribution, and modification are likely to influence  
448 disease progression (19, 40, 41). More work is required to elucidate biophysical  
449 differences between cell surface retained- and exo-GXM.

450 We identified genes that play a role in exo-GXM release. Deletion of *L/V7*, which  
451 decreases virulence in mice, reduces exo-GXM release in mild or non-capsule inducing  
452 growth medium, but does not affect capsule thickness. It has been previously  
453 demonstrated that *L/V7* is important for virulence and likely functions in Golgi transport

454 (42, 44). In contrast, deletion of the gene *IMA1* increased virulence in mice, potentially  
455 by increasing exo-GXM release under strong capsule inducing conditions without  
456 affecting capsule thickness. We used these two exo-GXM mutants as tools to  
457 investigate the biological importance of exo-GXM independent of surface capsule.

458 The *liv7Δ* mutant was identified as having a competitive disadvantage in a pool of  
459 gene deletion mutants (42), which would be surprising for a cell-extrinsic factor such as  
460 exo-GXM, whose effects might be muted in a competitive assay. The *ima1Δ* mutant was  
461 not found to have altered virulence in this screen. One interpretation is that *LIV7* has an  
462 unidentified phenotype in addition to exo-GXM release that impacts virulence. However,  
463 *liv7Δ* cells did not exhibit any significant ( $|Z| \geq 2.5$ ) phenotype when grown in the  
464 presence of over 150 different small molecules in a chemical-genetics screen (58).  
465 Other interpretations could include that individual fungal cells end up in separate  
466 sections of the lungs, or phagocytosed by different macrophages, etc., creating  
467 localized infection conditions where one mutant might not mask the phenotype of  
468 another. Each pool screened by Liu *et al.* contained, on average, more than one  
469 capsule deficient mutant (42), which would also lower the total exo-GXM levels.

470 Ours is not the first study connecting varied exo-GXM release with virulence.  
471 Analysis of a virulence-associated transcriptional network map previously revealed a  
472 positive correlation with *in vitro* exo-GXM release and mouse lung infectivity over 7 days  
473 (59). However, the transcription factor mutants also had altered surface capsule  
474 thickness, which may have influenced infectivity (59). Deletion of the flippase encoding  
475 gene *APT1* also resulted in reduced *in vitro* exo-GXM release despite wild-type surface  
476 capsule. The knockout was hypovirulent, but in contrast to our mutants, had reduced

477 surface capsule thickness *in vivo* (60). Our results support these previous findings, and  
478 provide a clearer link between exo-GXM and virulence because they do not suffer  
479 alterations to any additional virulence factors that we screened. Our data also provide  
480 additional support for a model in which regulated release of exo-GXM enhances  
481 virulence independent of surface capsule.

482 In a murine infection model, we showed a correlation between elevated *in vitro*  
483 exo-GXM levels, fungal burden and poor host survival. Exo-GXM levels also vary  
484 considerably amongst humans suffering from cryptococcal meningoencephalitis, with  
485 increased exo-GXM levels predictive of a non-protective Th2 immune signature and  
486 increased mortality (32, 61). These correlations suggest that perturbing exo-GXM  
487 release by cryptococcal cells appreciably affects the progression infection, since  
488 differences between wild-type- and *liv7Δ*-infected are apparent in mid- to late, not early,  
489 infection (**Fig. 5C**). Work on both *Aspergillus fumigatus* and *Candida albicans* have  
490 demonstrated that mutant strains capable of disease initiation are not necessarily  
491 capable of establishing robust disease (62). The opposite is also true: genes necessary  
492 for later disease might not have a defect in the initial establishment of infection (63). We  
493 propose that exo-GXM is more likely involved in establishment and dissemination,  
494 rather than disease initiation. We also established a positive correlation of exo-GXM  
495 release with biofilm adherence, suggesting that exo-GXM release during environmental  
496 growth may be important for promoting community level structure and adherence. It  
497 would not be surprising for there to be additional functions for exo-GXM in  
498 environmental settings.

499     Interestingly, exo-GXM also correlated with changes in cell body and capsule  
500 size distributions in the lungs. In *C. neoformans* infected animals, fungal cell body size  
501 and capsule thickness decreased over the course of infection, as exo-GXM levels  
502 increased. Correspondingly, increased GXM levels in the mouse lungs positively  
503 correlated with an increased frequency of smaller cells at an early time point in  
504 dissemination. *C. neoformans* cells in the brain and other extrapulmonary organs are  
505 much smaller than the lungs (**Fig. 6B** and (46, 50, 54)), suggesting that the emergence  
506 of smaller cells in the lungs is an important step in dissemination. The addition of  
507 purified GXM to *C. neoformans* cells growing in capsule-inducing media was sufficient  
508 to decrease cell body size and capsule thickness in a growth-dependent manner (**Fig.**  
509 **7**). These data suggest that exo-GXM may actually provide a concentration-dependent  
510 signal to *C. neoformans* cells that reduces cell size and capsule thickness. In the lungs,  
511 this mechanism may be a contributing factor in the generation of small cells with a  
512 greater propensity for dissemination.

513     These data raise the question of how *C. neoformans* cells might sense a polymer  
514 that also covers its cell surface. Since GXM is modified by O-acetylation (41) and can  
515 contain different branching structures (36), one possibility is that exo-GXM and cell  
516 surface GXM are differentially modified and that the fungal cell senses these  
517 modifications, then responds by mechanisms similar to two-component signal  
518 transduction systems in bacteria. This will be an area of future study. Overall, our  
519 results suggest that exo-GXM is an actively secreted virulence factor that may influence  
520 cell morphology to facilitate dissemination, and is capable of distally suppressing  
521 immune infiltration into the brain.

522 There is large body of literature demonstrating immunosuppressive properties for  
523 GXM (19). We focused on the brain, as cryptococcal meningoencephalitis is the leading  
524 cause of death in cryptococcosis patients, and is characterized by low levels of  
525 inflammation (9). Here, we observed that deleting a gene required for wild-type levels of  
526 exo-GXM release *in vitro* (*LIV7*) altered the host immune response to *C. neoformans*  
527 brain infection. Mice infected with *liv7Δ* cells had increased macrophages and  
528 neutrophils infiltrating the brain, compared to wild-type infected mice. Furthermore,  
529 administration of purified GXM was sufficient to reduce brain infiltrating immune cells in  
530 the context of acapsular *C. neoformans* infection. Our data suggest that removing exo-  
531 GXM from infected patients by antibody treatment could aid cryptococcosis treatment.

532

### 533 **Funding information**

534 This work was supported by a startup grant from the Pathology Department at the  
535 University of Utah to J.C.S.B. and NIH R01 NS041249 to T.E.L.

536

### 537 **Methods:**

538 Conditioned media collection: *C. neoformans* cells were cultured overnight in  
539 YNB+2%glucose at 30 °C before subculturing 1:100 in the desired medium. Culture  
540 OD<sub>600</sub> readings were taken 24 hours later and were normalized to the lowest measured  
541 OD<sub>600</sub>. Cells were pelleted by centrifugation at 3000xg for 5 min. The supernatant was  
542 collected and passed through a 0.22 µm filter, yielding conditioned media.

543 The following growth media were used in this study: YPAD (20g/L bacto-peptone,  
544 10g/L bacto-yeast extract, 2% glucose, 0.4g/L adenine sulfate). YPD (20g/L bacto-

Accepted Manuscript Posted Online  
Infection and Immunity  
[AI]  
peptone, 10g/L bacto-yeast extract, 2% glucose); YNB (Difco REF 291940) + 2%  
545 glucose; 25% YNB + 2% glucose; Low iron media (LIM) (5g/L asparagine, 0.4g/L  
546 K<sub>2</sub>HPO<sub>4</sub>, 0.1g MgSO<sub>4</sub>·7H<sub>2</sub>O, 0.5mg/L thiamine, 0.029mg/L boric acid, 1.88mg/L  
547 CuSO<sub>4</sub>·5H<sub>2</sub>O, 0.36mg/L MnCl<sub>2</sub>·4H<sub>2</sub>O, 0.021mg/L ZnCl<sub>2</sub>, 0.18mg/L NaMoO<sub>4</sub>·2H<sub>2</sub>O,  
548 0.05mg/L CaCl<sub>2</sub>·2H<sub>2</sub>O, 0.05mM bathophenanthroline disulfonic acid (BPDS), 1mM  
549 EDTA, 2% glucose, 50mM MOPS pH 6.0), 10% Sabouraud's dextrose (Difco REF  
550 238230) buffered with 50mM HEPES pH 8.0, HEPES pH 7.3, MOPS pH 6.0, or MES pH  
551 5.0; YCB (Difco REF 239110) + 5g/L urea; YCB + 0.5g/L urea.

553

554 Conditioned media blots: 10 µl of conditioned media collected from *C. neoformans*  
555 cultures were loaded into a 0.6% agarose gel and run at 33V for 18-20 hours at 0.5X  
556 TBE. The gels were processed with a 10 minute depurination rinse in a 0.25M HCl  
557 solution, followed by a 30 minute denaturation incubation in a 1.5M NaCl/0.5M NaOH  
558 solution, and a 30 minute neutralization incubation in 1.5M NaCl/0.5M Tris-HCl, pH 7.5.  
559 The gels were rinsed in distilled water following each incubation. Gel contents were  
560 subsequently transferred to a positively charged membrane using a standard Southern  
561 blot protocol with 10X SSC (saline-sodium citrate) in the reservoir. After overnight  
562 transfer, the blots were soaked briefly in 2X SSC and dried. Blots were then blocked for  
563 1 hour in 1X PBS+5% milk and incubated shaking overnight at 4 °C in 1X PBS+5% milk  
564 with 1:40,000 anti-GXM monoclonal antibody. The following morning, blots were rinsed  
565 3 times in 1X PBS, incubated 2 hours in 1X PBS+5% milk with 1:2500 goat anti-mouse  
566 HRP antibody, and washed for 2.5 hours in 1X PBS+0.1% tween-20, changing the wash  
567 buffer every 20 minutes. For imaging, blots were developed with Clarity Western ECL

568 substrate (BioRad Cat. 170-5061) and imaging on a BioRad Western Blot Imager. Anti-  
569 GXM monoclonal antibodies used in this study: F12D2, 1326 (Thomas Kozel, University  
570 of Nevada, Reno).

571

572 Cell measurements: *C. neoformans* cells collected from laboratory media were spun  
573 down at 3000xg for 5 min, washed twice in 1X PBS and resuspended in 1X PBS. To  
574 collect cells from infected mouse organs, 1 mL of organ homogenate was passed  
575 through a 70 µm cell strainer (Fisher Cat. No. 22-363-548). At this junction, capsule  
576 measurement methods were the same for both laboratory-grown and mouse-isolated *C.*  
577 *neoformans* cells. Cells were fixed for 15 minutes in 2% paraformaldehyde before  
578 washing twice with 1X PBS, and resuspending in 100 µl of 1X PBS. 4 µl of cell  
579 suspension was mixed with 4 µl of india ink (Higgins No. 44201) on a microscope slide,  
580 coverslipped and visualized. Successive, representative pictures were taken from the  
581 outside of the coverslipped area toward the middle, because smaller cells tended to  
582 spread towards the edges of the coverslip more so than larger cells. Total cell diameter  
583 was measured as the distance from one edge of the capsule to the opposite edge.

584 Cell body diameter was measured as the distance from one edge of the cell wall to the  
585 opposite edge. Capsule thickness was calculated as the total cell diameter, minus the  
586 cell body diameter, and divided by two; (total cell diameter–cell body diameter)/2.

587

588 Screen for exo-GXM mutants: Cells were spotted from 96 well frozen stocks to  
589 omnitrays containing YPD agar, then grown for 48 hours at 30°C. Colonies are used to  
590 inoculate deepwell plates containing 1 ml yeast nitrogen base (YNB) per well. Deepwell

591 plates were grown at 37°C for 48 hours with shaking (280 rpm). 10 µl of YNB culture  
592 were then used to inoculate 10% Sabouraud's (pH 7.3) cultures, which were then grown  
593 at 37°C for 48 hours with shaking. After growth, all cultures, either YNB or 10%  
594 Sabouraud's, pH 7.3, were harvested by centrifugation, then the supernatant was  
595 collected and stored for analysis.

596 We analyzed exo-GXM in YNB supernatants by dot blotting 4 µl of supernatant  
597 into each well of a dot blotter containing positively charged nylon membrane pre-soaked  
598 in 2X SSC, then applying vacuum. Membranes were air dried, then blocked and  
599 incubated with anti-GXM F12D2 antibody using standard procedures (see Materials and  
600 Methods section: *Conditioned media blots*). 10% Sabouraud's conditioned media  
601 samples were run on agarose gels and transferred to nylon membranes (see Materials  
602 and Methods section: *Conditioned media blots*).

603 Once we identified mutants with altered exo-GXM levels (decreased in YNB  
604 cultures or increased in 10% Sabouraud's, pH 7.3 cultures, we grew all mutants in 10%  
605 Sabouraud's, pH 7.3, then measured capsule thickness. Mutants with decreased cell  
606 surface capsule thickness (approximately 25% decrease compared to wild-type cells)  
607 were eliminated from further analysis. We then repeated the growth and exo-GXM blot  
608 for each strain. We normalized for cell density (to account for slow growing mutants),  
609 filtered the conditioned medium through a 0.22 µm filter to remove cells, and ran 10 µl  
610 of conditioned medium on an agarose gel using the procedure described in (see  
611 Materials and Methods section: *Conditioned media blots*). Finally, we stained for  
612 exposure of PAMPs such as chitin and mannoprotein (see Materials and Methods  
613 section: *Lectin Staining*) and removed mutants with increased exposure.

614

615 Lectin Staining: Cells grown for 24 hours in the appropriate media were pelleted,  
616 washed twice in 1X PBS and fixed for 12 minutes in 2% paraformaldehyde. Cells were  
617 then washed twice in 1X PBS and resuspended in 1X PBS. To an aliquot of cells, wheat  
618 germ agglutinin (WGA) conjugated to fluorescein (Vector Labs Cat. No. FL-1021) was  
619 added to a final concentration of 5 µg/ml, and incubated 30 minutes at room  
620 temperature with shaking. At the end of the WGA incubation, concanavalin A (ConA)  
621 conjugated to rhodamine (Vector Labs Cat. No. RL-1002) was added to a final  
622 concentration of 50 µg/ml. Cells were wash once in 1X PBS and imaged immediately.

623

624 Melanization and urease secretion: Cells grown overnight in YNB were washed twice in  
625 1X PBS and resuspended to a final concentration of  $2.5 \times 10^6$  cells/mL in 1X PBS. 10µl of  
626 cell suspension was spotted onto L-DOPA containing agar or Christensen's urea agar  
627 (Sigma 27048). Plates were checked daily for changes in melanization (brown/black  
628 colonies on L-DOPA), and urease secretion (pink coloration surrounding colonies on  
629 Christensen's urea).

630

631 GXM purification: GXM was purified as described previously (30). Briefly, 100 mL C.  
632 *neoformans* cells were cultured in YNB+2%glucose for 5 days at 30°C. Cultures were  
633 centrifuged at 12,000xg for 15min and the supernatant collected. Polysaccharides were  
634 precipitated from the supernatant overnight with the addition of 3 volumes of 95% EtOH  
635 at 4 °C. The solution was then centrifuged at 15,000xg for one hour, resuspended in  
636 0.2M NaCl and sonicated. After sonication, 3mg hexadecyltrimethylammonium bromide

637 (CTAB) (Fisher Cat. No. 227160) per 1 mg precipitate was slowly added to the solution  
638 on low heat. After removing from heat, another 2.5 volumes of 0.5mg CTAB was added.  
639 The solution was centrifuged at 11,000xg for 2 hours, and the pellet washed in 10%  
640 EtOH to remove any remaining CTAB. After an additional centrifugation at 18,000xg,  
641 the pellet was resuspended in 1M NaCl and sonicated for 2 hours. Once the GXM was  
642 solubilized, it was dialyzed (3.5kDa cutoff) versus sterile distilled water and then  
643 lyophilized. Purified, lyophilized GXM was stored at -80°C for subsequent use.

644

645 Adherence assay: We used a slightly modified protocol of biofilm formation and 2,3-Bis-  
646 (2-Methoxy-4-Nitro-5-Sulfophenyl)-2H-Tetrazolium-5-Carboxanilide (XTT) analysis, as  
647 described previously (48, 49). Briefly, 5 mL cultures were grown overnight in  
648 YNB+2%glucose at 30 °C, pelleted, washed in 1X PBS, and resuspended in 1X PBS.  
649 Cells were counted on a hemocytometer, diluted to  $10^7$  cells/mL in the appropriate  
650 media and plated in 100  $\mu$ l volumes in 96  $\mu$ l polystyrene plates (avoiding edge wells).  
651 Sterile media was plated as a negative control. Plates were incubated for 48 hours at  
652 37 °C to allow for adherence and biofilm maturation. Plates were then washed 3 times  
653 with 200  $\mu$ l of 1X PBS+0.05% tween-20 using a BioTek 405 TS microplate washer set  
654 to an intermediate flow rate. To determine the relative levels of cells that remained after  
655 washing, we used the XTT reduction assay to quantitate metabolic activity as a proxy  
656 for viable cell density. After plate washing, 100  $\mu$ l of a solution containing 0.5g/L XTT  
657 (Fisher Cat. No. X6493) and 4  $\mu$ M menadione (Sigma Cat. No. 58-27-5) in acetone in  
658 1X PBS was added to each well. Menadione was added to fresh XTT solution

659 immediately prior to adding the solution to a plate. Plates were incubated for 5 hours  
660 before moving 80  $\mu$ l supernatant aliquots to a new plate to read absorbance at 490nm.

661

662 **Mice:** For the intranasal infection model, we used ~8-week-old female C57BL/6NJ mice  
663 (Jackson Labs). *C. neoformans* cells were harvested from overnight 30°C YPD cultures,  
664 washed two times in 1X PBS, resuspended in 1X PBS, and then counted with a  
665 hemocytometer to determine the inoculum. Mice were anesthetized with  
666 ketamine/dexdomitor (mg/g) intraperitoneally before suspending them on horizontally  
667 tied thread by their front incisors. Mice were kept warm with a heat lamp and inoculated  
668 intranasally with  $2.5 \times 10^4$  *C. neoformans* cells in 50  $\mu$ l 1X PBS. After 10 minutes, mice  
669 were removed from thread and administered the reversal agent antisedan  
670 (~0.0125mg/g) intraperitoneally. For survival analyses, mice were weighed daily and  
671 euthanized by CO<sub>2</sub> asphyxiation and cervical dislocation, when they lost 15% of their  
672 initial mass. Mice used to analyze fungal burden, capsule size, and GXM levels were  
673 euthanized by the same measures at designated time points. Mice used for flow  
674 cytometry analysis were anesthetized with isoflurane and intracardially perfused with  
675 cold 1X PBS before cervical dislocation and brain extraction.

676 For the intracranial infection model, we used ~6-week-old female C57BL/6NJ  
677 mice (Jackson labs). *C. neoformans* inoculum was prepared as described above. Prior  
678 to inoculation, mice were anesthetized with ketamine/dexdomitor, as above. Mice were  
679 inoculated intracranially with 200 *C. neoformans* cells in 30 $\mu$ l 1X PBS via a 26Gx1/2  
680 needle. Animals were then administered antisedan to speed recovery.

681

682     Fungal Burden: Organs were harvested from euthanized mice, placed on ice, and  
683     homogenized with a Tissue Master Homogenizer (Omni International) in 5 mL 1X PBS.  
684     Serial dilutions of organ homogenates were plated on Sabouraud's dextrose agar with  
685     10mg/mL gentamycin and 100 mg/mL carbenicillin, and stored at 30°C in the dark for  
686     three days. Resulting colony forming units (CFU) were then counted to determine fungal  
687     burden.

688

689     GXM ELISA: 500  $\mu$ l of the same mouse organ homogenate used for CFU counts and *C.*  
690     *neoformans* cell measurements was collected and spun down at 3,000g for 5 minutes.  
691     The supernatant was then passed through a 0.22  $\mu$ m filter to remove cells. GXM levels  
692     in the resulting were quantified using the ALPHA Cryptococcal Antigen enzyme  
693     immunoassay (IMMY Ref. CRY101). GXM purified from *C. neoformans* cultures was  
694     diluted to generate standard curves.

695

696     Histology: Perfused mouse brains were divided in half and fixed overnight in 4%  
697     paraformaldehyde. 8  $\mu$ m thick sagittal slices were mounted on microscope slides and  
698     stored at -20 °C. Successive sections were stained with hematoxylin and eosin or  
699     Grocott's methenamine silver (ThermoFisher Scientific Cat. No. 87008).

700

701     Flow cytometry: Perfused mouse brains were collected in RPMI, ground gently to  
702     disperse tissue and spun in a 90% Percoll (Sigma Cat. No. P1644) with a 63% Percoll  
703     underlay to isolate leukocytes at the interface. Leukocytes were resuspended in FACS  
704     buffer (1X PBS, 1% bovine serum albumin), and stained with the appropriate

705 fluorescently labeled antibodies. Labeled cells were fixed for 20 minutes in 4%  
706 paraformaldehyde before analysis on a LSRII Fortessa (BD Biosciences). Antibodies  
707 used in this study (eBiosciences): CD45-eFluor450 (48-0451-82), CD4-APC (Cat. No.  
708 17-0041-82), CD8-FITC (11-0081-82), F4/80-FITC (11-4801-82), Ly6G-FITC (11-5931-  
709 82), Ly6C-APC (17-5932-82).

710  
711 **References:**  
712

- 713 1. May RC, Stone NRH, Wiesner DL, Bicanic T, Nielsen K. 2016. Cryptococcus:  
714 from environmental saprophyte to global pathogen. *Nat Rev Micro* 14:106-117.
- 715 2. Goldman DL, Khine H, Abadi J, Lindenberg DJ, Pirofski L-a, Niang R, Casadevall  
716 A. 2001. Serologic Evidence for *Cryptococcus neoformans* Infection in Early  
717 Childhood. *Pediatrics* 107:e66-e66.
- 718 3. Garcia-Hermoso D, Janbon G, Dromer F. 1999. Epidemiological Evidence for  
719 Dormant *Cryptococcus neoformans* Infection. *Journal of Clinical Microbiology*  
720 37:3204-3209.
- 721 4. Idnurm A, Bahn Y-S, Nielsen K, Lin X, Fraser JA, Heitman J. 2005. Deciphering  
722 the Model Pathogenic Fungus *Cryptococcus Neoformans*. *Nat Rev Micro* 3:753-  
723 764.
- 724 5. Chen Y, Toffaletti DL, Tenor JL, Litvintseva AP, Fang C, Mitchell TG, McDonald  
725 TR, Nielsen K, Boulware DR, Bicanic T, Perfect JR. 2014. The *Cryptococcus*  
726 *neoformans* Transcriptome at the Site of Human Meningitis. *mBio* 5:e01087-13.
- 727 6. Rajasingham R, Smith RM, Park BJ, Jarvis JN, Govender NP, Chiller TM,  
728 Denning DW, Loyse A, Boulware DR. 2017. Global burden of disease of HIV-  
729 associated cryptococcal meningitis: an updated analysis. *The Lancet Infectious  
730 Diseases* 17:873-881.
- 731 7. van de Beek D, de Gans J, Tunkel AR, Wijdicks EFM. 2006. Community-  
732 Acquired Bacterial Meningitis in Adults. *New England Journal of Medicine*  
733 354:44-53.
- 734 8. Kim JV, Kang SS, Dustin ML, McGavern DB. 2009. Myelomonocytic cell  
735 recruitment causes fatal CNS vascular injury during acute viral meningitis. *Nature*  
736 457:191-195.
- 737 9. Chuck SL, Sande MA. 1989. Infections with *Cryptococcus neoformans* in the  
738 Acquired Immunodeficiency Syndrome. *New England Journal of Medicine*  
739 321:794-799.
- 740 10. Robertson EJ, Najjuka G, Rolfe MA, Akampurira A, Jain N, Anantharanj J, von  
741 Hohenberg M, Tassieri M, Carlsson A, Meya DB, Harrison TS, Fries BC,  
742 Boulware DR, Bicanic T. 2014. *Cryptococcus neoformans* Ex Vivo Capsule Size  
743 Is Associated With Intracranial Pressure and Host Immune Response in HIV-  
744 associated Cryptococcal Meningitis. *The Journal of Infectious Diseases* 209:74-  
745 82.

- 746 11. Olszewski MA, Noverr MC, Chen G-H, Toews GB, Cox GM, Perfect JR,  
747 Huffnagle GB. 2004. Urease Expression by *Cryptococcus neoformans* Promotes  
748 Microvascular Sequestration, Thereby Enhancing Central Nervous System  
749 Invasion. *The American Journal of Pathology* 164:1761-1771.
- 750 12. Jarvis JN, Meintjes G, Bicanic T, Buffa V, Hogan L, Mo S, Tomlinson G, Kropf P,  
751 Noursadeghi M, Harrison TS. 2015. Cerebrospinal Fluid Cytokine Profiles Predict  
752 Risk of Early Mortality and Immune Reconstitution Inflammatory Syndrome in  
753 HIV-Associated Cryptococcal Meningitis. *PLoS Pathogens* 11:e1004754.
- 754 13. Boulware DR, Bonham SC, Meya DB, Wiesner DL, Park GS, Kambugu A, Janoff  
755 EN, Bohjanen PR. 2010. Paucity of Initial Cerebrospinal Fluid Inflammation in  
756 Cryptococcal Meningitis is associated with subsequent Immune Reconstitution  
757 Inflammatory Syndrome. *The Journal of infectious diseases* 202:962-970.
- 758 14. Zaragoza O, Nielsen K. 2013. Titan cells in *Cryptococcus neoformans*: Cells with  
759 a giant impact. *Current opinion in microbiology* 16:409-413.
- 760 15. O'Meara TR, Alspaugh JA. 2012. The *Cryptococcus neoformans* Capsule: a  
761 Sword and a Shield. *Clinical Microbiology Reviews* 25:387-408.
- 762 16. Doering TL. 2009. How Sweet it is! Cell Wall Biogenesis and Polysaccharide  
763 Capsule Formation in *Cryptococcus neoformans*. *Annual review of microbiology*  
764 63:223-247.
- 765 17. Zaragoza O, Taborda CP, Casadevall A. 2003. The efficacy of complement-  
766 mediated phagocytosis of *Cryptococcus neoformans* is dependent on the  
767 location of C3 in the polysaccharide capsule and involves both direct and  
768 indirectC3-mediated interactions. *European Journal of Immunology* 33:1957-  
769 1967.
- 770 18. Zaragoza O, Chrisman CJ, Castelli MV, Frases S, Cuenca-Estrella M,  
771 Rodríguez-Tudela JL, Casadevall A. 2008. Capsule enlargement in  
772 *Cryptococcus neoformans* confers resistance to oxidative stress suggesting a  
773 mechanism for intracellular survival. *Cellular microbiology* 10:2043-2057.
- 774 19. Vecchiarelli A, Pericolini E, Gabrielli E, Kenno S, Perito S, Cenci E, Monari C.  
775 2013. Elucidating the immunological function of the *Cryptococcus neoformans*  
776 capsule. *Future Microbiology* 8:1107-1116.
- 777 20. Vecchiarelli A, Retini C, Monari C, Tascini C, Bistoni F, Kozel TR. 1996. Purified  
778 capsular polysaccharide of *Cryptococcus neoformans* induces interleukin-10  
779 secretion by human monocytes. *Infection and Immunity* 64:2846-2849.
- 780 21. Monari C, Bistoni F, Casadevall A, Pericolini E, Pietrella D, Kozel TR,  
781 Vecchiarelli A. 2005. Glucuronoxylomannan, a Microbial Compound, Regulates  
782 Expression of Costimulatory Molecules and Production of Cytokines in  
783 Macrophages. *The Journal of Infectious Diseases* 191:127-137.
- 784 22. Retini C, Kozel TR, Pietrella D, Monari C, Bistoni F, Vecchiarelli A. 2001.  
785 Interdependency of Interleukin-10 and Interleukin-12 in Regulation of T-Cell  
786 Differentiation and Effector Function of Monocytes in Response to Stimulation  
787 with *Cryptococcus neoformans*. *Infection and Immunity* 69:6064-6073.
- 788 23. Vecchiarelli A, Retini C, Pietrella D, Monari C, Tascini C, Beccari T, Kozel TR.  
789 1995. Downregulation by cryptococcal polysaccharide of tumor necrosis factor  
790 alpha and interleukin-1 beta secretion from human monocytes. *Infection and*  
791 *Immunity* 63:2919-2923.

- 792 24. Retini C, Vecchiarelli A, Monari C, Bistoni F, Kozel TR. 1998. Encapsulation of  
793 Cryptococcus neoformans with Glucuronoxylomannan Inhibits the Antigen-  
794 Presenting Capacity of Monocytes. *Infection and Immunity* 66:664-669.
- 795 25. Vecchiarelli A, Pietrella D, Lupo P, Bistoni F, McFadden DC, Casadevall A. 2003.  
796 The polysaccharide capsule of Cryptococcus neoformans interferes with human  
797 dendritic cell maturation and activation. *Journal of Leukocyte Biology* 74:370-378.
- 798 26. Villena SN, Pinheiro RO, Pinheiro CS, Nunes MP, Takiya CM, DosReis GA,  
799 Previato JO, Mendonça-Previato L, Freire-de-Lima CG. 2008. Capsular  
800 polysaccharides galactoxylomannan and glucuronoxylomannan from  
801 Cryptococcus neoformans induce macrophage apoptosis mediated by Fas ligand.  
802 *Cellular Microbiology* 10:1274-1285.
- 803 27. Ellerbroek PM, Hoepelman AIM, Wolbers F, Zwaginga JJ, Coenjaerts FEJ. 2002.  
804 Cryptococcal Glucuronoxylomannan Inhibits Adhesion of Neutrophils to  
805 Stimulated Endothelium In Vitro by Affecting Both Neutrophils and Endothelial  
806 Cells. *Infection and Immunity* 70:4762-4771.
- 807 28. Dong ZM, Murphy JW. 1995. Intravascular cryptococcal culture filtrate (CneF)  
808 and its major component, glucuronoxylomannan, are potent inhibitors of  
809 leukocyte accumulation. *Infection and Immunity* 63:770-778.
- 810 29. Dong ZM, Murphy JW. 1996. Cryptococcal polysaccharides induce L-selectin  
811 shedding and tumor necrosis factor receptor loss from the surface of human  
812 neutrophils. *Journal of Clinical Investigation* 97:689-698.
- 813 30. Cherniak R, Morris LC, Anderson BC, Meyer SA. 1991. Facilitated isolation,  
814 purification, and analysis of glucuronoxylomannan of Cryptococcus neoformans.  
815 *Infection and Immunity* 59:59-64.
- 816 31. Jarvis JN, Percival A, Bauman S, Pelfrey J, Meintjes G, Williams GN, Longley N,  
817 Harrison TS, Kozel TR. 2011. Evaluation of a Novel Point-of-Care Cryptococcal  
818 Antigen Test on Serum, Plasma, and Urine From Patients With HIV-Associated  
819 Cryptococcal Meningitis. *Clinical Infectious Diseases: An Official Publication of*  
820 *the Infectious Diseases Society of America* 53:1019-1023.
- 821 32. Scriven JE, Graham LM, Schutz C, Scriba TJ, Wilkinson KA, Wilkinson RJ,  
822 Boulware DR, Urban BC, Laloo DG, Meintjes G. 2016. A Glucuronoxylomannan-  
823 Associated Immune Signature, Characterized by Monocyte Deactivation and an  
824 Increased Interleukin 10 Level, Is a Predictor of Death in Cryptococcal Meningitis.  
825 *The Journal of Infectious Diseases* 213:1725-1734.
- 826 33. Buchanan KL, Murphy JW. 1998. What makes Cryptococcus neoformans a  
827 pathogen? *Emerging Infectious Diseases* 4:71-83.
- 828 34. Frases S, Nimrichter L, Viana NB, Nakouzi A, Casadevall A. 2008. Cryptococcus  
829 neoformans Capsular Polysaccharide and Exopolysaccharide Fractions Manifest  
830 Physical, Chemical, and Antigenic Differences. *Eukaryotic Cell* 7:319-327.
- 831 35. Yoneda A, Doering TL. 2008. Regulation of Cryptococcus neoformans Capsule  
832 Size Is Mediated at the Polymer Level. *Eukaryotic Cell* 7:546-549.
- 833 36. Cordero RJB, Frases S, Guimarães AJ, Rivera J, Casadevall A. 2011. Evidence  
834 for Branching in Cryptococcal Capsular Polysaccharides and Consequences on  
835 its Biological Activity. *Molecular microbiology* 79:1101-1117.
- 836 37. de S. Araújo GR, Fontes GN, Leão D, Rocha GM, Pontes B, Sant'Anna C, de  
837 Souza W, Frases S. 2016. Cryptococcus neoformans capsular polysaccharides

- Accepted Manuscript Posted Online  
Infection and Immunity  
[AI] Infection and Immunity
- 838 form branched and complex filamentous networks viewed by high-resolution  
 839 microscopy. *Journal of Structural Biology* 193:75-82.
- 840 38. Kozel TR, Levitz SM, Dromer F, Gates MA, Thorkildson P, Janbon G. 2003.  
 841 Antigenic and Biological Characteristics of Mutant Strains of *Cryptococcus*  
 842 *neoformans* Lacking Capsular O Acetylation or Xylosyl Side Chains. *Infection*  
 843 and *Immunity* 71:2868-2875.
- 844 39. Urai M, Kaneko Y, Ueno K, Okubo Y, Aizawa T, Fukazawa H, Sugita T, Ohno H,  
 845 Shibuya K, Kinjo Y, Miyazaki Y. 2015. Evasion of Innate Immune Responses by  
 846 the Highly Virulent *Cryptococcus gattii* by Altering Capsule  
 847 Glucuronoxylomannan Structure. *Frontiers in Cellular and Infection Microbiology*  
 848 5:101.
- 849 40. Ellerbroek PM, Lefeber DJ, van Veghel R, Scharringa J, Brouwer E, Gerwig GJ,  
 850 Janbon G, Hoepelman AIM, Coenjaerts FEJ. 2004. O-Acetylation of  
 851 Cryptococcal Capsular Glucuronoxylomannan Is Essential for Interference with  
 852 Neutrophil Migration. *The Journal of Immunology* 173:7513.
- 853 41. Janbon G, Himmelreich U, Moyrand F, Improvisi L, Dromer F. 2001. Cas1p is a  
 854 membrane protein necessary for the O-acetylation of the *Cryptococcus*  
 855 *neoformans* capsular polysaccharide. *Molecular Microbiology* 42:453-467.
- 856 42. Liu OW, Chun CD, Chow ED, Chen C, Madhani HD, Noble SM. 2008.  
 857 Systematic genetic analysis of virulence in the human fungal pathogen  
 858 *Cryptococcus neoformans*. *Cell* 135:174-188.
- 859 43. Willment JA, Brown GD. 2008. C-type lectin receptors in antifungal immunity.  
 860 *Trends in Microbiology* 16:27-32.
- 861 44. Brown JCS, Madhani HD. 2012. Approaching the Functional Annotation of  
 862 Fungal Virulence Factors Using Cross-Species Genetic Interaction Profiling.  
 863 *PLOS Genetics* 8:e1003168.
- 864 45. Bojarczuk A, Miller KA, Hotham R, Lewis A, Ogryzko NV, Kamuyango AA, Frost  
 865 H, Gibson RH, Stillman E, May RC, Renshaw SA, Johnston SA. 2016.  
 866 *Cryptococcus neoformans* Intracellular Proliferation and Capsule Size  
 867 Determines Early Macrophage Control of Infection. *Scientific Reports* 6:21489.
- 868 46. Rivera J, Feldmesser M, Cammer M, Casadevall A. 1998. Organ-Dependent  
 869 Variation of Capsule Thickness in *Cryptococcus neoformans* during Experimental  
 870 Murine Infection. *Infection and Immunity* 66:5027-5030.
- 871 47. Martinez LR, Casadevall A. 2015. Biofilm Formation by *Cryptococcus*  
 872 *neoformans*. *Microbiology Spectrum* 3.
- 873 48. Martinez LR, Casadevall A. 2005. Specific Antibody Can Prevent Fungal Biofilm  
 874 Formation and This Effect Correlates with Protective Efficacy. *Infection and*  
 875 *Immunity* 73:6350-6362.
- 876 49. Pierce CG, Uppuluri P, Tristan AR, Wormley FL, Mowat E, Ramage G, Lopez-  
 877 Ribot JL. 2008. A simple and reproducible 96 well plate-based method for the  
 878 formation of fungal biofilms and its application to antifungal susceptibility testing.  
 879 *Nature protocols* 3:1494-1500.
- 880 50. Trevijano-Contador N, Rueda C, Zaragoza O. 2016. Fungal morphogenetic  
 881 changes inside the mammalian host. *Seminars in Cell & Developmental Biology*  
 882 57:100-109.

- 883 51. Ballou ER, Johnston SA. 2017. The cause and effect of Cryptococcus  
884 interactions with the host. *Current Opinion in Microbiology* 40:88-94.
- 885 52. Vidal JE, Boulware DR. 2015. Lateral Flow Assay for Cryptococcal Antigen: an  
886 Important Advance to Improve the Continuum of HIV Care and Reduce  
887 Cryptococcal Meningitis-Related Mortality. *Revista do Instituto de Medicina  
888 Tropical de São Paulo* 57:38-45.
- 889 53. García-Barbazán I, Trevijano-Contador N, Rueda C, de Andrés B, Pérez-Tavárez  
890 R, Herrero-Fernández I, Gaspar ML, Zaragoza O. 2016. The formation of titan  
891 cells in *Cryptococcus neoformans* depends on the mouse strain and correlates  
892 with induction of Th2-type responses. *Cellular Microbiology* 18:111-124.
- 893 54. Okagaki LH, Strain AK, Nielsen JN, Charlier C, Baltes NJ, Chrétien F, Heitman J,  
894 Dromer F, Nielsen K. 2010. Cryptococcal Cell Morphology Affects Host Cell  
895 Interactions and Pathogenicity. *PLoS Pathogens* 6:e1000953.
- 896 55. Zaragoza O, García-Rodas R, Nosanchuk JD, Cuenca-Estrella M, Rodríguez-  
897 Tudela JL, Casadevall A. 2010. Fungal Cell Gigantism during Mammalian  
898 Infection. *PLoS Pathogens* 6:e1000945.
- 899 56. Reese AJ, Doering TL. 2003. Cell wall α-1,3-glucan is required to anchor the  
900 *Cryptococcus neoformans* capsule. *Molecular Microbiology* 50:1401-1409.
- 901 57. Rodrigues ML, Nimrichter L, Oliveira DL, Frases S, Miranda K, Zaragoza O,  
902 Alvarez M, Nakouzi A, Feldmesser M, Casadevall A. 2007. Vesicular  
903 Polysaccharide Export in *Cryptococcus neoformans* Is a Eukaryotic Solution to  
904 the Problem of Fungal Trans-Cell Wall Transport. *Eukaryotic Cell* 6:48-59.
- 905 58. Brown JCS, Nelson J, VanderSluis B, Deshpande R, Butts A, Kagan S,  
906 Polacheck I, Krysan DJ, Myers CL, Madhani HD. 2014. Unraveling the biology of  
907 a fungal meningitis pathogen using chemical genetics. *Cell* 159:1168-1187.
- 908 59. Maier EJ, Haynes BC, Gish SR, Wang ZA, Skowyra ML, Marulli AL, Doering TL,  
909 Brent MR. 2015. Model-driven mapping of transcriptional networks reveals the  
910 circuitry and dynamics of virulence regulation. *Genome Research* 25:690-700.
- 911 60. Rizzo J, Oliveira DL, Joffe LS, Hu G, Gazos-Lopes F, Fonseca FL, Almeida IC,  
912 Frases S, Kronstad JW, Rodrigues ML. 2014. Role of the Apt1 Protein in  
913 Polysaccharide Secretion by *Cryptococcus neoformans*. *Eukaryotic Cell* 13:715-  
914 726.
- 915 61. Boulware DR, von Hohenberg M, Rolfs MA, Bahr NC, Rhein J, Akampurira A,  
916 Williams DA, Taseera K, Schutz C, McDonald T, Muzoora C, Meintjes G, Meya  
917 DB, Nielsen K, Huppler Hullsieck K. 2016. Human Immune Response Varies by  
918 the Degree of Relative Cryptococcal Antigen Shedding. *Open Forum Infectious  
919 Diseases* 3:ofv194.
- 920 62. Saville SP, Lazzell AL, Monteagudo C, Lopez-Ribot JL. 2003. Engineered  
921 Control of Cell Morphology In Vivo Reveals Distinct Roles for Yeast and  
922 Filamentous Forms of *Candida albicans* during Infection. *Eukaryotic Cell* 2:1053-  
923 1060.
- 924 63. Beattie SR, Mark KMK, Thammahong A, Ries LNA, Dhingra S, Caffrey-Carr AK,  
925 Cheng C, Black CC, Bowyer P, Bromley MJ, Obar JJ, Goldman GH, Cramer RA.  
926 2017. Filamentous fungal carbon catabolite repression supports metabolic  
927 plasticity and stress responses essential for disease progression. *PLOS  
928 Pathogens* 13:e1006340.

- 929 64. Lipovsky MM, Tsenova L, Coenjaerts FEJ, Kaplan G, Cherniak R, Hoepelman  
930 AIM. 2000. Cryptococcal glucuronoxylomannan delays translocation of  
931 leukocytes across the blood–brain barrier in an animal model of acute bacterial  
932 meningitis. Journal of Neuroimmunology 111:10-14.  
933  
934

935 **Figure Legends**

936 **Figure 1: Levels of detectable exo-GXM negatively correlate with capsule  
937 thickness under a variety of media conditions.** To generate conditioned media, we  
938 normalized 24 hour cultures by cell density, then passed the supernatants through a  
939 0.22  $\mu$ m filter to remove fungal cells. **(A)** Representative image of cell/capsule  
940 measurements used in this study. **(B)** We tested supernatants for free GXM (“exo-GXM”)  
941 by blotting and probing with the F12D2 anti-GXM mAb. See Materials and Methods for  
942 further details. A representative blot showing relative levels of exo-GXM collected from  
943 cells cultured for 24 hours under a variety of capsule and non-capsule inducing  
944 conditions. **(C)** Intensity of exo-GXM bands relative to YNB+2% glucose exo-GXM (blue  
945 bars) were quantitated for three independent experiments and plotted next to absolute  
946 measurements of capsule thickness (yellow bars) (n=30 cells). Data was combined from  
947 three independent experiments. Bars represent the mean and error bars represent the  
948 standard deviation (SD).

949  
950 **Figure 2: Identification of a genetic mutant (*liv7 $\Delta$* ) with reduced exo-GXM release,  
951 but no observable changes to capsule thickness. **(A)** Representative india ink  
952 images of cells grown in 10% Sabouraud's dextrose pH 7.3 for 24 hours. Capsule  
953 thickness was similar across KN99 wild-type (WT) cells, and cells from each  
954 independent *liv7* deletion strain (*liv7 $\Delta$ #1 and *liv7 $\Delta$ #2*) **(B)** Quantification of cell body***

955 diameter and capsule thickness from three independent experiments (n=30 cells per  
956 strain; bars represent mean with SD). **(C)** Conditioned media from wild-type and mutant  
957 cultures grown in weak-capsule inducing conditions (YNB+2% glucose) for 24 hours.  
958 Blots were probed with anti-GXM antibody F12D2. **(D)** Quantification of blot signal  
959 intensities shows reduced exo-GXM release by *liv7Δ#1* / *liv7Δ#2* cells. Data was  
960 combined from three independent experiments. P-values were calculated using a Mann-  
961 Whitney test; bars represent mean with SD. **(E)** Conditioned media from wild-type and  
962 mutant cultures grown in mild-capsule inducing conditions (YCB+0.5g/L urea) for 24  
963 hours. Blots were probed with anti-GXM antibody F12D2. **(F)** Quantification of blot  
964 signal intensities shows reduced exo-GXM release by *liv7Δ#1* / *liv7Δ#2* cells under mild-  
965 capsule inducing conditions. Data was combined from three independent experiments.  
966 P-values were calculated using a Mann-Whitney test; bars represent mean with SD. **(G)**  
967 Two-fold less GXM by mass was purified from *liv7Δ#1* / *liv7Δ#2* cells when compared to  
968 wild-type cells grown for 72 hours in YNB+2% glucose. **(H)** Purified GXM from wild-type  
969 and *liv7Δ#1* / *liv7Δ#2* cells was resuspended at a concentration of 1mg/mL and  
970 immunoblotted with mAb F12D2. **(I)** Quantification of signal intensities from the blot in  
971 (H) shows similar intensity for GXM purified from wild-type and *liv7Δ#1* / *liv7Δ#2* cells.  
972

973 **Figure 3: Identification of a genetic mutant (*ima1Δ*) with increased exo-GXM**  
974 **release, but no observable changes to capsule thickness. (A)** Representative india  
975 ink images of cells grown in 10% Sabouraud's dextrose pH 7.3 for 24 hours. Capsule  
976 thickness was similar across KN99 wild-type (WT) cells, and cells from each  
977 independent *ima1* (also *cnag\_00658*, see main text for details) deletion strain (*ima1Δ#1*

and *ima1Δ#2*). **(B)** Quantification of cell body diameter and capsule thickness from three independent experiments (n=30 cells per strain; bars represent mean with SD) **(C)** Conditioned media from cultures grown for 24 hours under strong capsule-inducing conditions (10% Sabouraud's, pH 7.3). Blots were probed with anti-GXM antibody F12D2. **(D)** Quantification of blot signal intensities shows increased exo-GXM release by *ima1Δ#1 / ima1Δ#2* (Combined data from three independent experiments). P-values were calculated using a Mann-Whitney test; bars represent mean with SD. **(E)** Conditioned media from cultures grown for 24 hours under non-capsule-inducing conditions (YNB+2% glucose). Blots were probed with anti-GXM antibody F12D2. **(F)** Quantification of blot signal intensities shows similar exo-GXM release by *ima1Δ#1 / ima1Δ#2*, when compared to wild-type cells (Combined data from three independent experiments). P-values were calculated using a Mann-Whitney test; bars represent mean with SD.

**Figure 4: Mutants' alterations to exo-GXM release correlates with adherence.**  $10^6$  *C. neoformans* cells were seeded into individual wells of 96-well polystyrene plates and incubated at 37°C. 48 hours later, the wells were washed to remove non-adhered and/or weakly adhered cells before resuspension in XTT for colorimetric analysis of metabolic activity as a proxy for viable cell count. **(A)** OD<sub>490</sub> readings from cells grown in YNB, normalizing to wild-type cell readings. *liv7Δ#1 / #2* cell adherence was reduced and *ima1Δ#1 / #2* cell adherence was increased when compared to wild-type cells. **(B)** OD<sub>490</sub> readings from cells grown in 10% Sabouraud's pH 7.3, normalizing to wild-type cell readings. *ima1Δ#1 / #2* cell adherence was increased when compared to wild-type

1001 cells. Combined data from three independent experiments. P-values were calculated  
1002 using a Mann-Whitney test; bars represent mean with SD. **(C)** OD<sub>490</sub> readings from cells  
1003 grown in YNB, normalizing to wild-type cell readings. Cells were mixed with purified  
1004 GXM or vehicle (PBS) prior to inoculating plates. Wild-type and *liv7Δ#1 / #2* cell  
1005 adherence increased in the presence of GXM.

1006

1007 **Figure 5: Mutants' alterations to *in vitro* exo-GXM release correlate with changes**  
1008 **in survival and fungal burden during infection. (A)** C57BL/6NJ mice inoculated  
1009 intranasally with *ima1Δ#1 / #2* (n=10 and n=10, respectively) reach endpoint  
1010 significantly sooner than wild-type infected mice (n=15). Wild-type infected mice  
1011 reached endpoint sooner than *liv7Δ#1 / #2* (n=8 and n=14, respectively) infected mice.  
1012 Mock infected animals given sterile 1X PBS (n=5) did not show signs of disease 35  
1013 days post-inoculation. P-values were calculated using a Log-rank (Mantel-Cox) Test. **(B)**  
1014 *liv7Δ#1 / #2* infected mice (n=8 and n=8, respectively) show decreased lung burden  
1015 beginning at 10 days post-inoculation compared to wild-type (n=12). **(C)** Brain fungal  
1016 burden is significantly lower in *liv7Δ#1 / #2* infected animals when compared to wild-type.  
1017 **(D)** Lung fungal burden is significantly higher in *ima1Δ#1 / #2* (n=8 and n=8,  
1018 respectively) infected mice than wild-type infected mice (n=8 on days 3, 10, and 14;  
1019 n=12 on day 16) beginning at least 3 days post-inoculation. **(E)** Dissemination to the  
1020 brain trends higher in *ima1Δ#1 / #2* infected mice. P-values were calculated using a  
1021 Mann-Whitney test.

1022

1023 **Figure 6: Cell size distributions over the course of infection.** We visualized fungal  
1024 cells from tissue homogenates (from infected mice in **Fig. 5B-E**) in india ink and  
1025 measured cell size. Total diameter = cell + capsule diameter (**Fig 1A**). **(A)** Mean total  
1026 cell diameter decreases over time within the lungs of wild-type infected mice as the  
1027 population shifts toward smaller cells with smaller capsules (n=3-4 mice per time point,  
1028 ≥120 cells per mouse). **(B)** Disseminated cells found in the brain late in infection (20 dpi)  
1029 overlay with the size profile of smaller cells found in the lungs at the same time point. **(C)**  
1030 **and D)** Early after inoculation (3 dpi) the distributions of both **(C)** *liv7Δ#1 / #2* and **(D)**  
1031 *ima1Δ#1 / #2* cells match that of wild-type in the lungs (n=3 mice, ≥50 cells per mouse).  
1032 **(E and F)** At an early point in dissemination (14 dpi), **(E)** *liv7Δ#1 / #2* cell populations  
1033 were of larger average total cell diameter than wild-type *C. neoformans* cells in the  
1034 lungs. **(F)** *ima1Δ#1 / #2* cells were of smaller average total cell diameter than wild-type  
1035 *C. neoformans* cells (n=4 mice, ≥120 cells per mouse). Frequency bin size = 2.0 μm. P-  
1036 values were calculated using a Mann-Whitney test.  
1037

1038 **Figure 7: Treatment with GXM decreases capsule thickness.** We induced cell  
1039 surface capsule by growing cells 24 hours in 10% Sabouraud's pH 7.3, then added  
1040 various concentrations of either **(A)** purified GXM or **(B)** conditioned medium from a  
1041 YNB-grown culture of wild-type (KN99) *C. neoformans* cells. We find a dosage-  
1042 dependent decrease in capsule thickness following exposure to both purified GXM and  
1043 conditioned medium. Histograms contain data from four separate experiments, with at  
1044 least 60 cells measured per condition for each experiment. We also observed a  
1045 decrease in cell size (see **Fig. S7**) with GXM or conditioned medium treatment. P-

1046 values were calculated using a Mann-Whitney test. Frequency bins sizes were 0.5  $\mu\text{m}$ .  
1047 Representative DIC images of **(C)** untreated cells or **(D)** cells treated with 50  $\mu\text{g}/\text{ml}$   
1048 GXM are shown.

1049

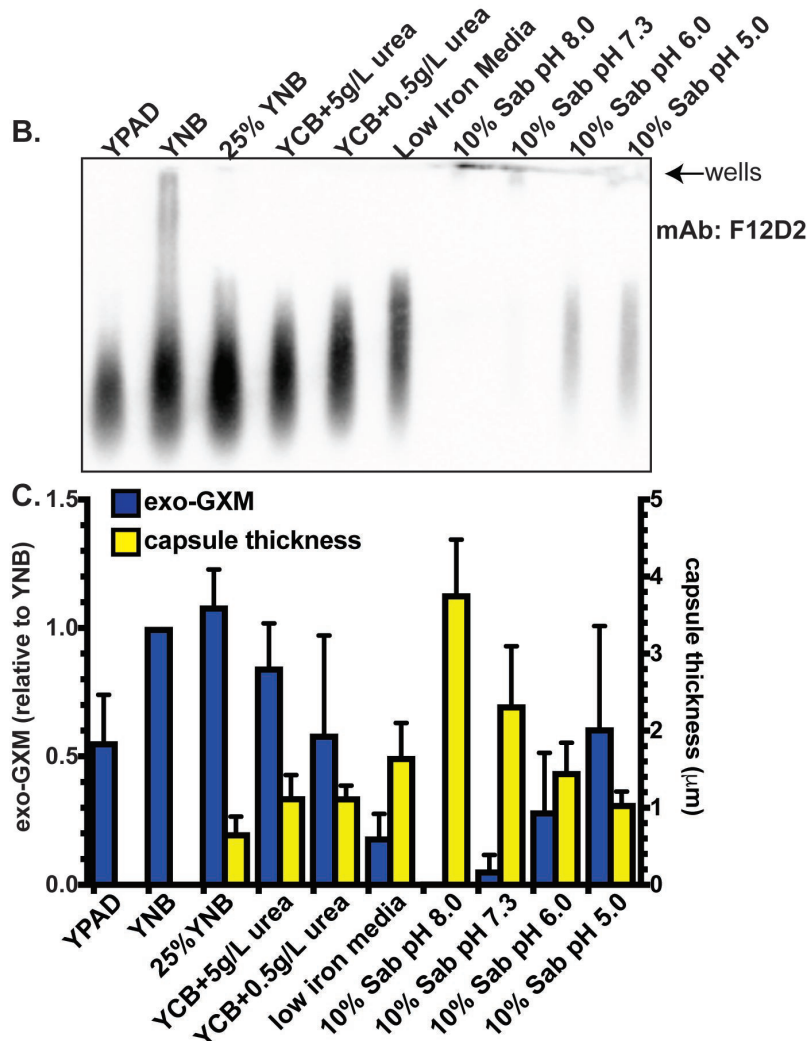
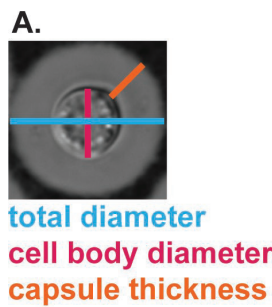
1050 **Figure 8: Mice infected with *liv7Δ* cells display increased innate immune infiltrate**  
1051 **in the brain.** Mouse brains were harvested late (20 dpi) in infection for flow cytometry  
1052 analysis of infiltrating immune cells. **(A)** CD4 $^{+}$  T cells are scarce in both wild-type and  
1053 *liv7Δ#1 / #2* infected brains. **(B)** CD8 $^{+}$  T cells show a significant increase over wild-type  
1054 in *liv7Δ#2* infected brains, but this was not replicated in *liv7Δ#1* infected brains **(C)**  
1055 Macrophages (CD45 $^{\text{hi}}$ F4/80 $^{+}$ ) and **(D)** neutrophils (CD45 $^{+}$ Ly6G $^{+}$ Ly6C $^{+}$ ) are significantly  
1056 increased in the brains of *liv7Δ#1* and *#2* as compared to wild-type and mock-infected  
1057 brains. P-values were calculated using a Mann-Whitney test; bars represent the median.

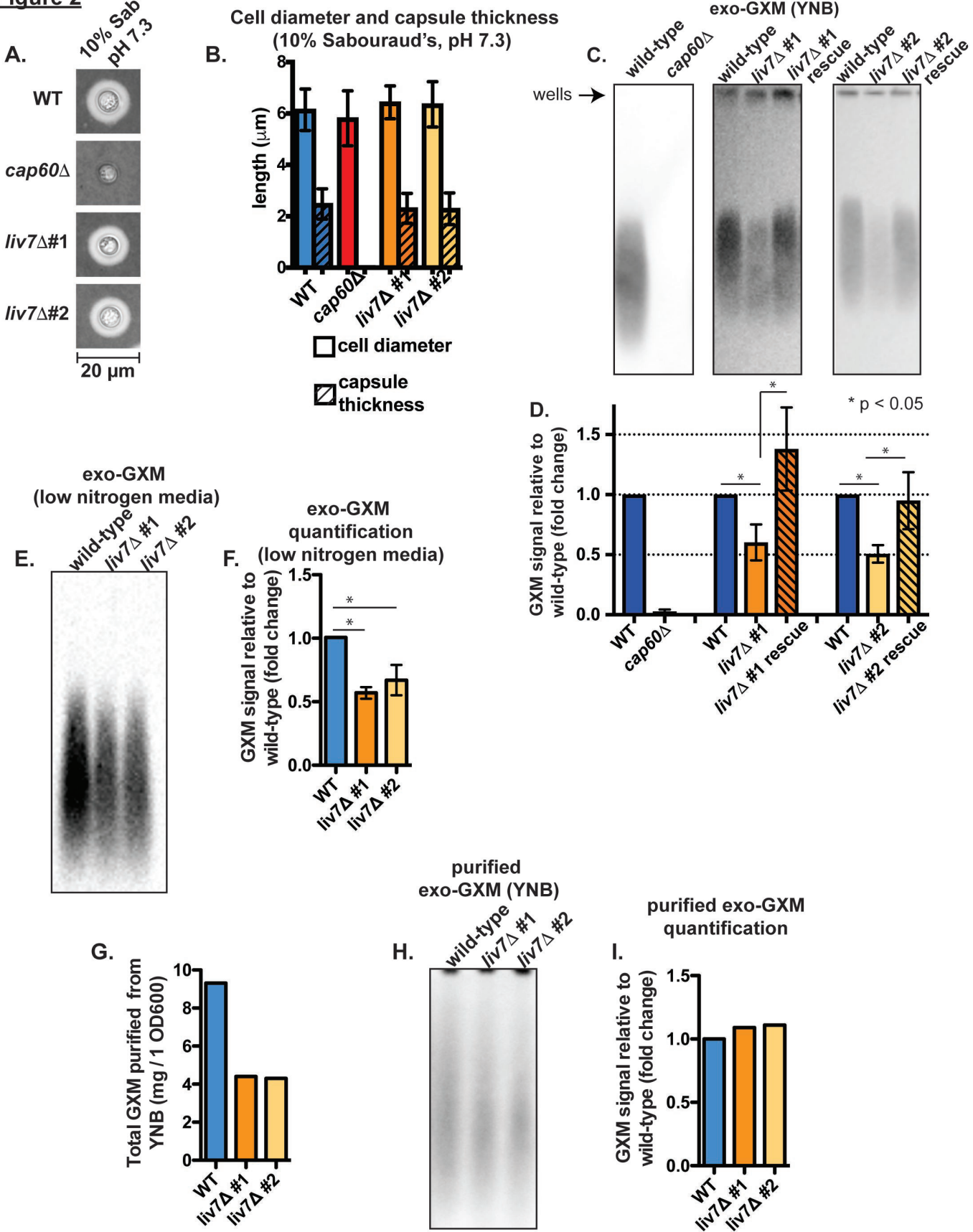
1058

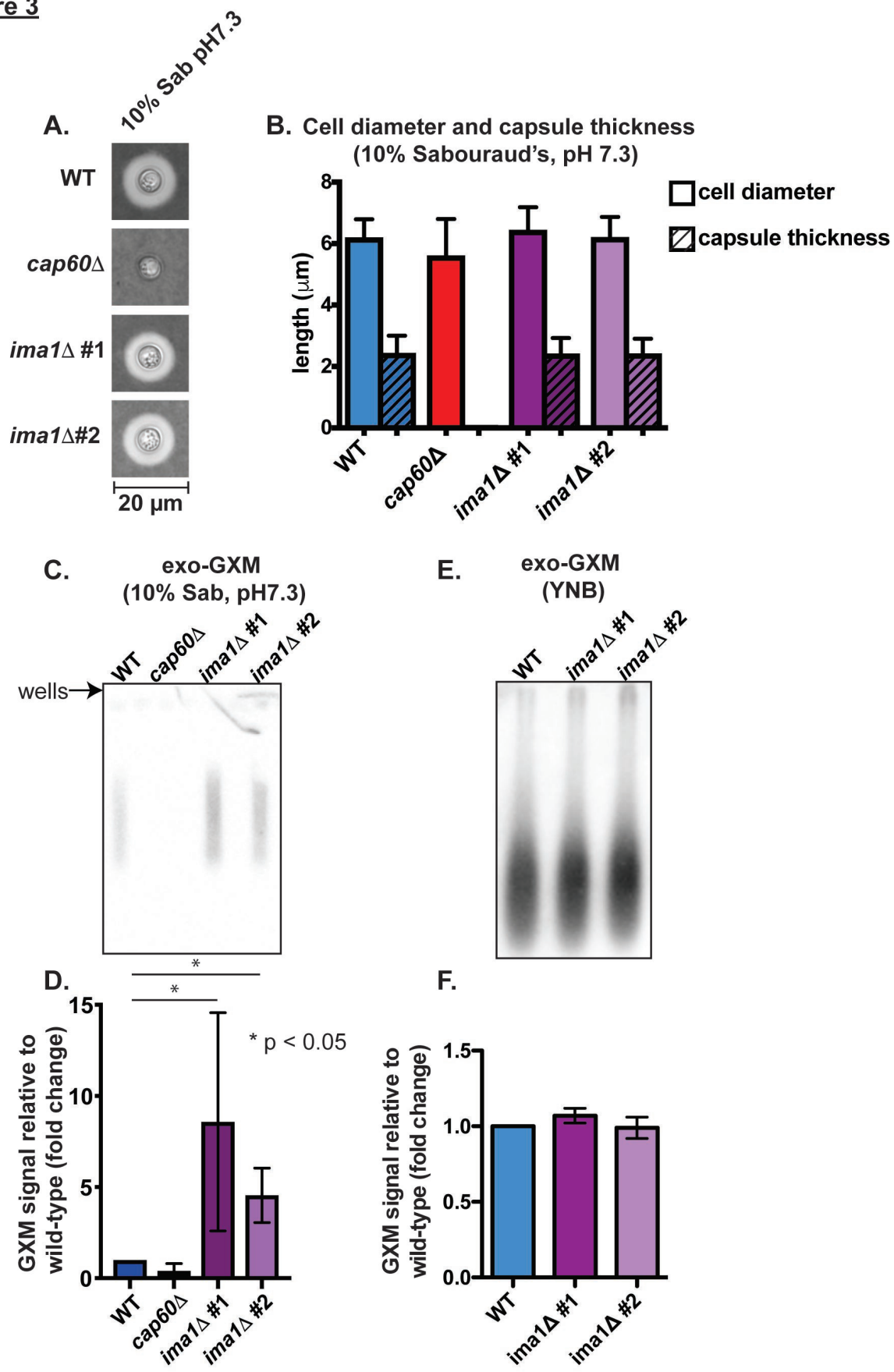
1059 **Figure 9: Purified GXM is sufficient to suppress immune infiltration into the brain**  
1060 **in response to inflammation-inducing acapsular (*cap60Δ*) *C. neoformans*.** 6-week-  
1061 old C57Bl/6NJ mice were intracranially inoculated with 200 *cap60Δ* fungal cells in 30  $\mu\text{l}$   
1062 1X PBS. Beginning 5 days prior to inoculation, mice were administered intraperitoneal  
1063 injections of either 200  $\mu\text{g}/\text{mL}$  GXM or 200  $\mu\text{l}$  sterile PBS. On the day of inoculation,  
1064 mice were administered this treatment intravenously to ensure GXM would be present  
1065 in the blood-stream. At 3 dpi brains were harvested to determine fungal burden by  
1066 colony forming unit counts. Separate mice were sacrificed to analyze infiltrating immune  
1067 cells by flow cytometry. **(A)** Diagram of experimental procedures. **(B)** Mice infected with  
1068 *cap60Δ* displayed increased brain immune infiltrate (CD45 $^{\text{hi}}$  cells) over wild-type

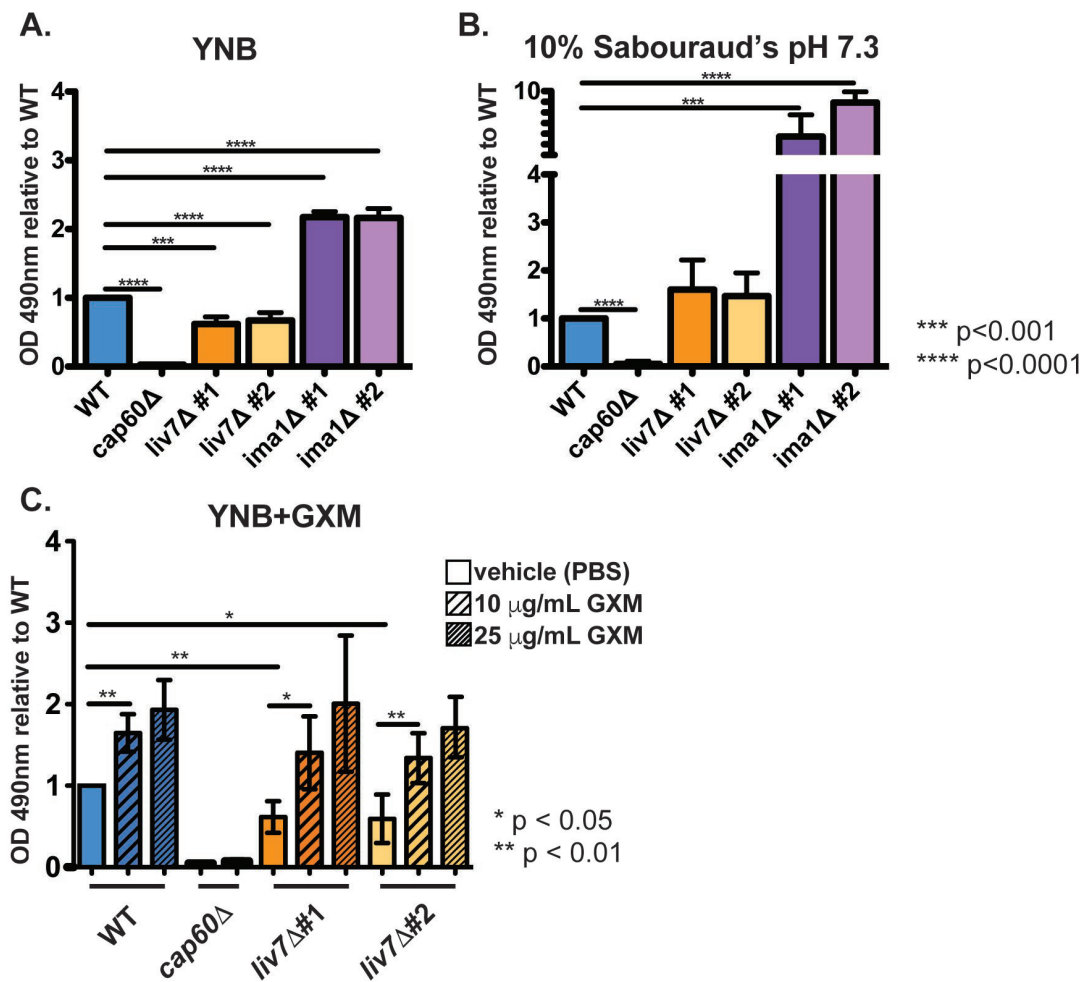
1069 infected mice. Immune infiltration into the brains of *cap60* $\Delta$  infected mice was reduced  
1070 with the administration of GXM. **(C)** Representative flow plots for data shown in **(B)**. **(D)**  
1071 Mice infected with wild-type KN99 cells suffered increased fungal brain burden when  
1072 compared to mice infected with *cap60* $\Delta$ . Administration of GXM had no significant effect  
1073 on wild-type fungal burden, but resulted in significantly increased *cap60* $\Delta$  fungal burden  
1074 compared to *cap60* $\Delta$ -infected mice that did not receive GXM. P-values were calculated  
1075 using a Mann-Whitney test; bars represent the median.

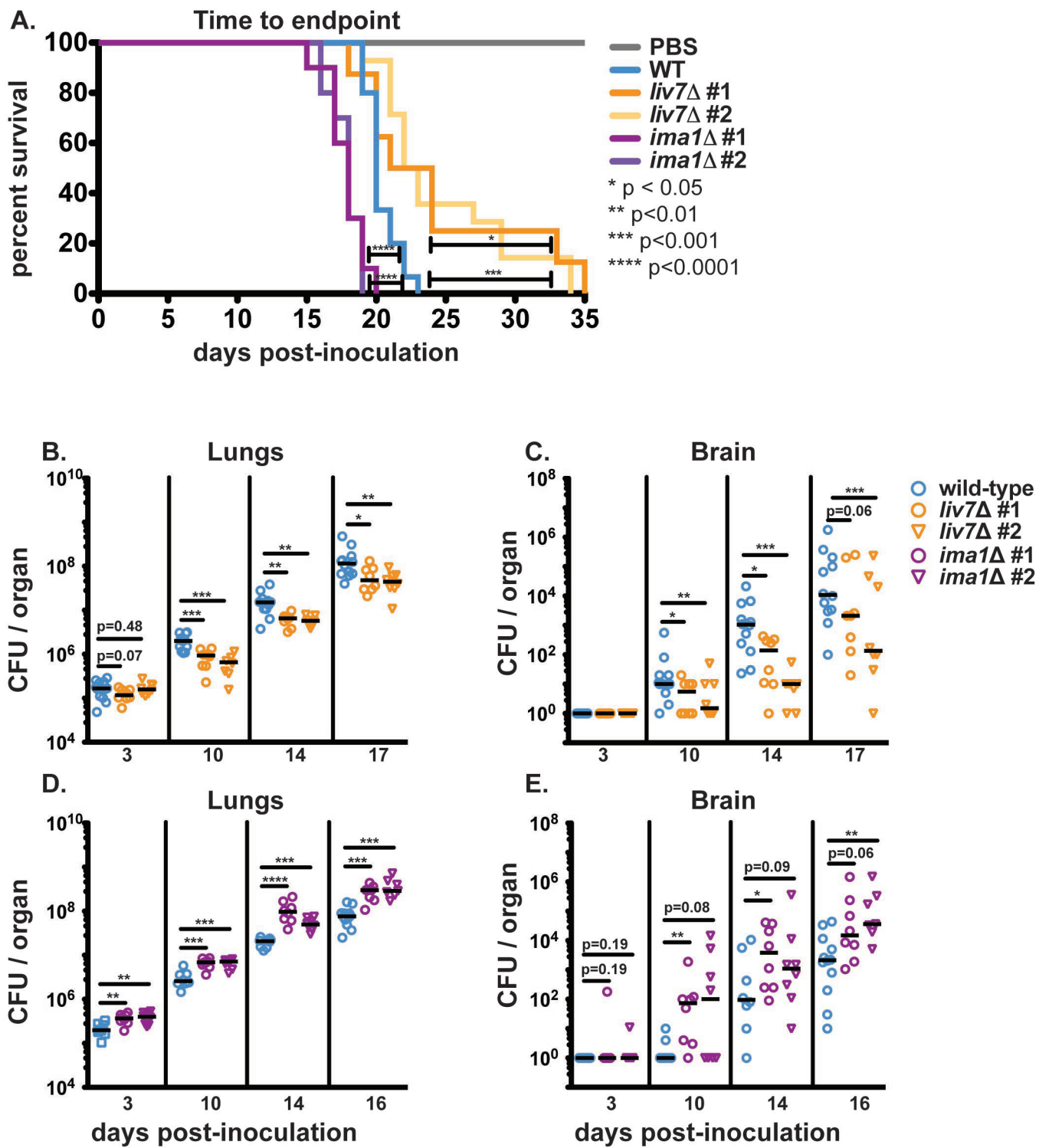
1076

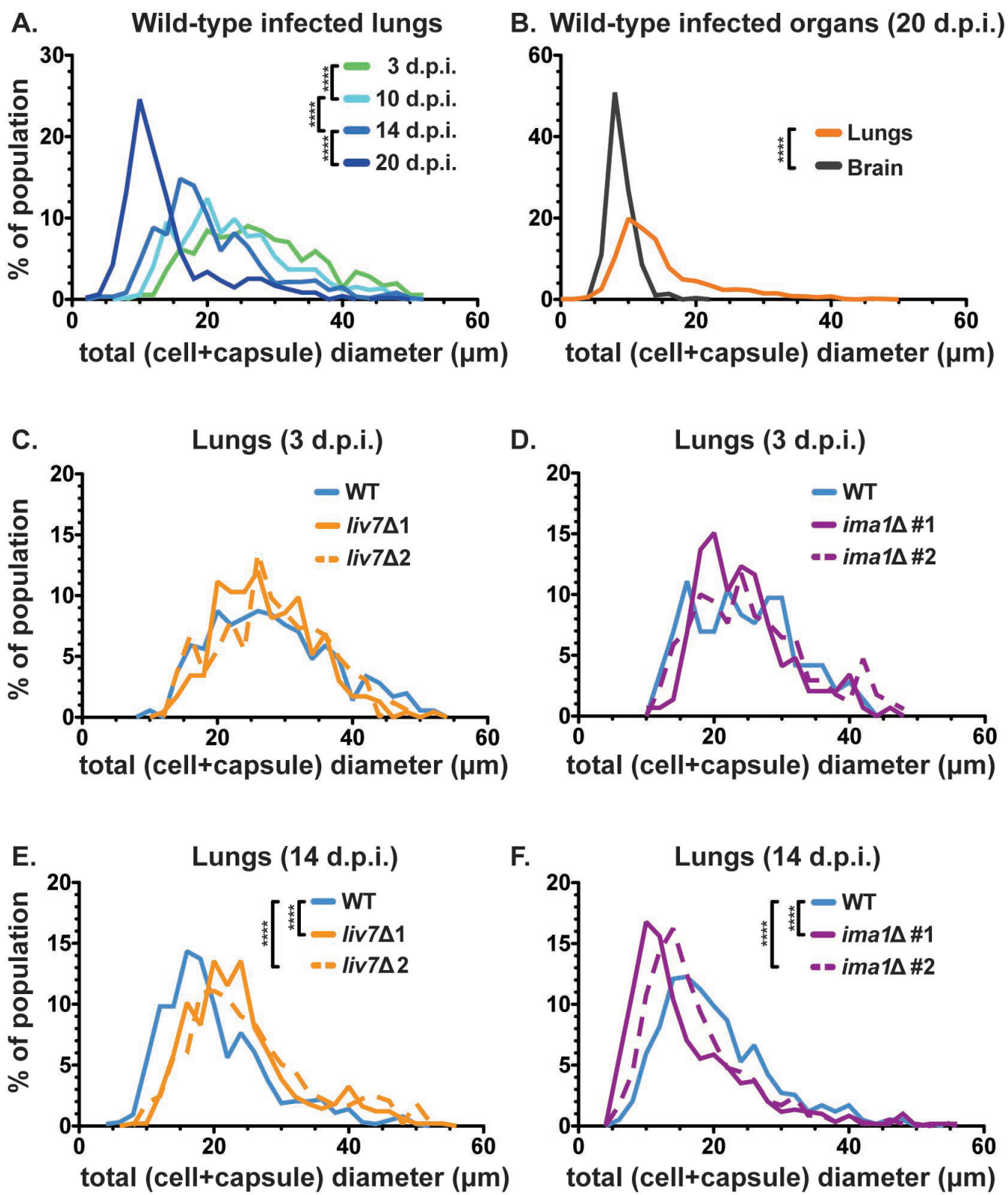
**Figure 1**

**Figure 2**

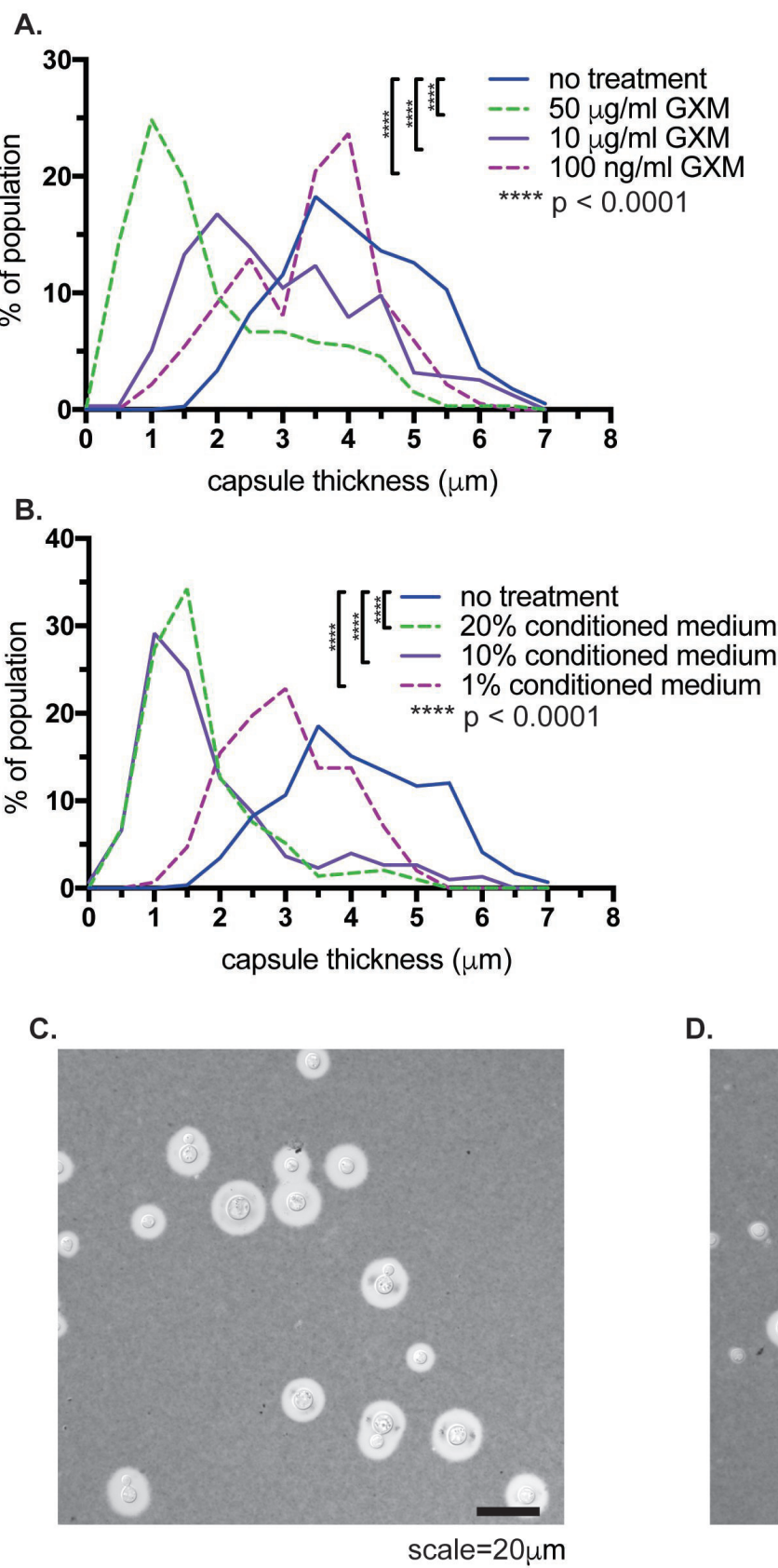
**Figure 3**

**Figure 4**

**Figure 5**

**Figure 6**

\*\*\*\* p &lt; 0.0001

**Figure 7**

**Figure 8**